CHAPTER

14

MAGNETOSPHERIC "KILLER" RELATIVISTIC ELECTRON DROPOUTS (REDs) AND REPOPULATION: A CYCLICAL PROCESS

Rajkumar Hajra*, Bruce T. Tsurutani†

French National Center for Scientific Research (CNRS), Orléans, France California Institute of Technology, Pasadena, CA, United States†*

CHAPTER OUTLINE

Extreme Events in Geospace. https://doi.org/10.1016/B978-0-12-812700-1.00014-5

1 INTRODUCTION

The Earth's magnetosphere is filled with energetic charged particles that gradient and curvature drift around the closed magnetic field region. These azimuthally drifting particles form part of the Earth's radiation belt known as the Van Allen belt (Van Allen and Frank, 1959; Vernov et al., 1960; Frank et al., 1963). The inner Van Allen belt ($1 \leq L < 3$) is composed of a combination of high-energy electrons ($\sim$100 keV) and very energetic protons ($\geq$10–100 MeV). The protons are produced by cosmic ray albedo neutron decay (CRAND: Singer, 1958; Dragt et al., 1966; Fennell et al., 2015; Selesnick, 2015; Selesnick et al., 2016; Su et al., 2016). The outer zone ($3 \leq L \leq 7$) is dominated by $\geq$100 keV electrons and $\sim$30–300 keV protons that are injected into the nightside magnetosphere by substorms and magnetic storms (e.g., Paulikas and Blake, 1979; Baker et al., 1979). The relativistic ($\geq$1 MeV) electrons are part of the outer belt, but their variability is not synchronous with those of the substorm and magnetic storm injected $\sim$10–100 keV electrons and $\sim$30–300 keV protons (Freeman, 1964; Paulikas and Blake, 1979; Baker et al., 1994; Friedel et al., 2002; Turner et al., 2014).

Understanding the cause and predicting the occurrence of these extremely energetic (relativistic) electrons in the Earth's outer belt are important because the particles cause hazards to Earth-orbiting spacecraft (Baker et al., 1994, 1998; Wrenn, 1995; Blake et al., 1997; Horne, 2003). The acceleration and decrease of the relativistic electrons are major aspects of extreme space weather effects. The electrons are known to be highly variable with orders of magnitude variations on time scales of a few minutes to several years. The variability depends on the solar cycle for long-term effects (Baker et al., 1986; Hajra et al., 2014c) and on solar wind and interplanetary variations for short-term effects (Tsurutani et al., 2006; Miyoshi and Kataoka, 2008, 2011; Kasahara et al., 2009; Baker et al., 2014; Hietala et al., 2014; Kilpua et al., 2015; Li et al., 2015).

The most important phase of the $\sim$11-year solar cycle for the acceleration of relativistic electrons is the declining phase (Paulikas and Blake, 1979; Baker et al., 1979, 1990; Li et al., 2001; Tsurutani et al., 2006). This is the interval where high-speed solar wind streams (HSSs) emanating from coronal holes (Sheeley et al., 1976) are dominant (see Tsurutani et al., 1995, 2006). In the HSSs, there are Alfvén wave trains (Belcher and Davis, 1971; Tsurutani and Gonzalez, 1987; Tsurutani et al., 1994, 1995) containing substantial and frequent southward interplanetary magnetic fields (IMFs) that lead to HILDCAA (high-intensity long-duration continuous auroral activity: Tsurutani and Gonzalez, 1987) events. HILDCAAs are intervals of continuous substorms and injection events (Tsurutani et al., 2004; Guarnieri, 2006; Hajra et al., 2013, 2014a; Souza et al., 2016; Mendes et al., 2017). There are only moderate intensity geomagnetic storms ($-50\ \text{nT} \geq \text{Dst} > -100\ \text{nT}$: Gonzalez et al., 1994) associated with corotating interaction regions (CIRs) during this phase of the solar cycle (Tsurutani et al., 1995).

During the solar cycle maximum, intense geomagnetic magnetic storms ($\text{Dst} < -100\ \text{nT}$) are induced by interplanetary coronal mass ejections (ICMEs) (see Tsurutani et al., 1988; Gonzalez et al., 1994; Chakraborty et al., 2008; Echer et al., 2008; Hajra et al., 2010; Hajra, 2011). Relativistic electron flux variability has been noted in and around these magnetic storm intervals (Baker et al., 1994; Li et al., 1997; Onsager et al., 2002; Horne et al., 2009). Although this phase of the solar cycle is less important from the overview of flux intensities, we will give a review of current hypotheses of loss and acceleration processes. We will also show one specific ICME storm interval for the reader.

Recently Tsurutani et al. (2016) proposed a new scenario for the relativistic electron dropout (RED) events that are not related to geomagnetic storms. These are caused by impingement of the

interplanetary heliospheric plasma sheet (HPS) onto the magnetosphere. It should be noted that HPSs are located in slow solar wind streams. The HPSs and heliospheric current sheets (HCS: Smith et al., 1978) occur prior to the CIRs and HSSs (Tsurutani et al., 2006, 2016). Hajra et al. (2013, 2014c, 2015a, b) reported that the long and intense auroral activity intervals of HILDCAAs lead to relativistic electron acceleration irrespective of whether geomagnetic storms precede. We will discuss these new results in some detail. These studies indicate the predictability of the magnetospheric relativistic electrons well in advance of their occurrence.

In the present chapter we will review the outer zone Van Allen relativistic electron variation as a cyclical process. First HPSs cause the depopulation of the electrons and then later the HSSs lead to the repopulation of the electrons.

2 SOLAR WIND/INTERPLANETARY DRIVING AND GEOMAGNETIC CHARACTERISTICS: A SCHEMATIC

Fig. 1 illustrates schematically the slow solar wind and the fast solar wind interaction, associated interplanetary structures, and resulting geomagnetic effects. The interaction between the slow solar wind (on the left of the Vsw panel) and the fast solar wind (HSS, on the right) results in an interaction region characterized by the high plasma densities (Nsw), high IMF intensities (Bo), and high plasma temperatures (not shown), known as the CIR (Smith and Wolfe, 1976).

The *vertical dashed line* in Fig. 1 indicates the HCS. The high-density region adjacent to the HCS is the HPS (Winterhalter et al., 1994). The HCS is a region where the IMF reverses its polarity, that is, from an inward polarity to an outward one, or vice versa (Ness and Wilcox, 1964; Smith et al., 1978). An HCS crossing is identified by a reversal of both Bx and By components of the IMF (in either GSM or GSE coordinate systems). The HCS is accompanied by neighboring high-density cold plasma, typical of the slow solar wind. The cold plasma has been called the HPS. It should be noted that the HPS is typically part of the slow solar wind. The HPS occurs prior to the CIR and HSS as the HPS is typically "swept up" by the HSS (Tsurutani et al., 1995, 2006, 2016).

Fig. 1 shows an example of the causes of relativistic electron decreases and repopulation. The HPSs impact the magnetosphere, depleting it of the relativistic electrons (Tsurutani et al., 2016). The HPSs compress both the magnetosphere and the preexisting ~10–100 keV energetic particles within it. The betatron-accelerated protons generate coherent electromagnetic ion cyclotron (EMIC) waves in the dayside outer magnetosphere through a temperature anisotropy ($T_\perp/T_\parallel > 1$) instability. The waves in turn interact with relativistic electrons and cause the rapid loss to the atmosphere before they reach the magnetopause. By the time the CIR reached the magnetosphere, the relativistic electrons had already been lost. It is not until the HSS interval that the relativistic electrons repopulated the magnetosphere (Hajra et al., 2015a). The HSSs are accompanied by embedded Alfvén waves. The waves are convected to 1 AU and beyond by the solar wind (Belcher and Davis, 1971; Tsurutani et al., 1994). The southward component of the Alfvén waves causes magnetic reconnection at the Earth's dayside magnetopause (Dungey, 1961; Gonzalez and Mozer, 1974; Tsurutani et al., 1995), leading to substorms and convection events and energetic ~10–100 keV electron injections into the nightside sector of the magnetosphere (DeForest and McIlwain, 1971; Horne and Thorne, 1998). The temperature anisotropy of the heated electrons leads to plasma instability (Brice, 1964; Kennel and Petschek, 1966; Tsurutani and

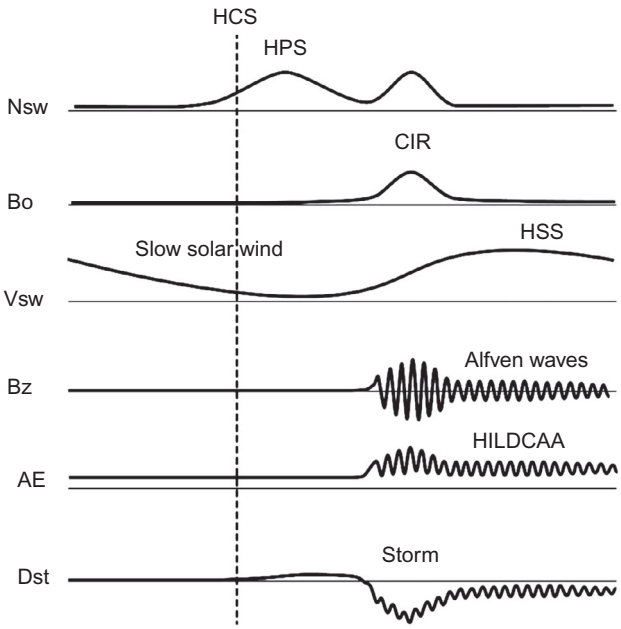

FIG. 1

A schematic of the slow stream-HSS interaction region. From top to bottom, the panels show: the solar wind density Nsw, the IMF magnitude Bo, the solar wind speed Vsw, the IMF Bz component, the geomagnetic AE, and Dst indices, respectively. The *dashed vertical line* indicates the HCS and the density associated with it (asymmetrically on the right side) is the HPS. A CIR and HSS HILDCAA are shown for context.

Modified from Tsurutani, B.T., Hajra, R., Tanimori, T., Takada, A., Bhanu, R., Mannucci, A.J., Lakhina, G.S., Kozyra, J.U., Shiokawa, K., Lee, L.C., Echer, E., Reddy, R.V., Gonzalez, W.D., 2016. Heliospheric plasma sheet (HPS) impingement onto the magnetosphere as a cause of relativistic electron dropouts (REDs) via coherent EMIC wave scattering with possible consequences for climate change mechanisms. J. Geophys. Res. 121, 10130–10156. doi: 10.1002/2016JA022499.

Lakhina, 1997), generating electromagnetic plasma waves called "chorus" (Tsurutani and Smith, 1977; Tsurutani et al., 1979, 2013; Inan et al., 1978; Meredith et al., 2001). Resonant interactions of the chorus waves with ~100 keV electrons lead to acceleration to relativistic energies (Inan et al., 1978; Horne and Thorne, 1998; Thorne et al., 2005, 2013; Summers et al., 2007; Reeves et al., 2013; Boyd et al., 2014).

The sporadic magnetic reconnection by the southward component of the interplanetary Alfvén wave train also results in the prolonged periods of intense auroral activity at Earth, which can last for days to weeks (Tsurutani et al., 1995, 2006; Gonzalez et al., 2006; Guarnieri, 2006; Kozyra et al., 2006; Turner et al., 2006; Hajra et al., 2013, 2014a,b, 2017). The auroral activity has been called HILDCAAs (Tsurutani and Gonzalez, 1987). By definition, HILDCAAs are characterized by peak AE intensity >1000 nT and a minimum duration of 2 days where AE never drops below 200 nT for >2 h at a time. Detailed studies of HILDCAA characteristics may be found in Hajra et al. (2013, 2014b). It was shown (Hajra et al., 2014c) that the lengthy and continuous intervals of AE activity are ideal for electron acceleration in the outer radiation belt.

3 RELATIVISTIC ELECTRON DROPOUT AND ACCELERATION: AN EXAMPLE

Fig. 2 shows an example of solar/interplanetary variations as well as geomagnetic and radiation belt effects during a HILDCAA event on September 15–20, 2003. This is taken and modified from Hajra et al. (2015b). The solar wind/interplanetary data were obtained from the OMNI database (http://omniweb.gsfc.nasa.gov/). These are time adjusted to take into account the solar wind convection time from the spacecraft to the bow shock. The IMFs are in the geocentric solar magnetospheric (GSM) coordinate system. The geomagnetic indices were obtained from the World Data Center for Geomagnetism, Kyoto, Japan (http://wdc.kugi.kyoto-u.ac.jp). The HILDCAA (denoted by the horizontal line in the AE panel) had a duration of ~5 days, from ~2102 UT on day 258 (September 15) to ~2203 UT on day 263 (September 20). The HILDCAA initiation was associated with a CIR, marked by the

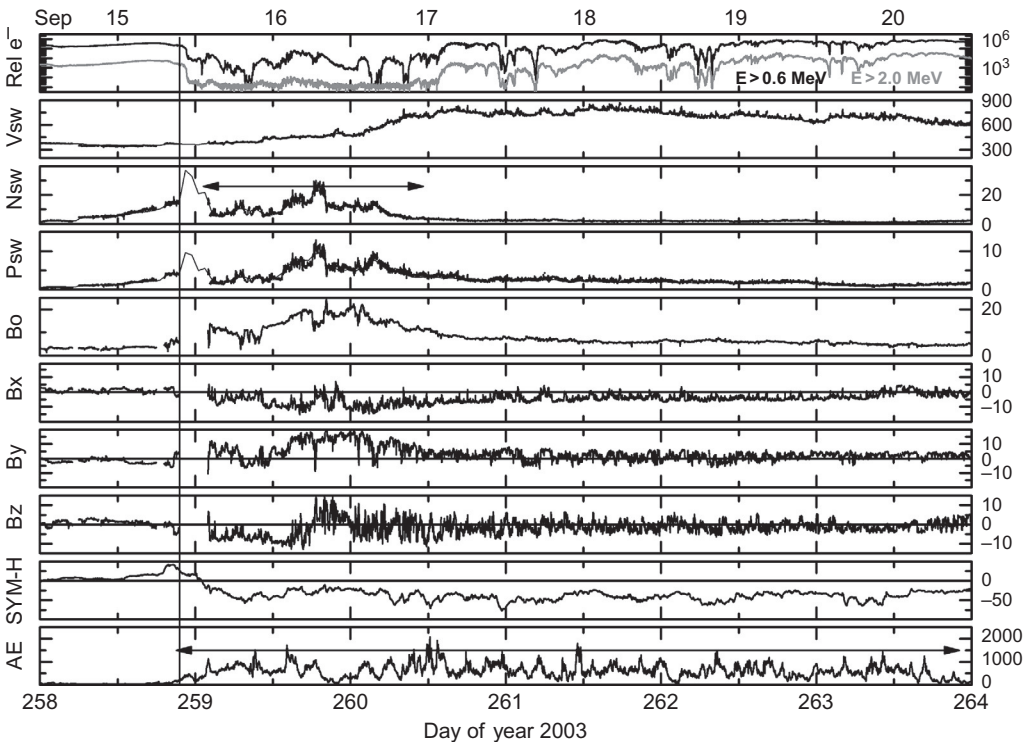

FIG. 2

HILDCAA event occurring on September 15–20, 2003. From top to bottom, the panels show the variations of $E>0.6$ *(black curve)* and $E>2.0$ MeV *(gray curve)* electron fluxes (FU) from GOES-8, solar wind speed (Vsw in km s^{-1}), plasma density (Nsw in cm^{-3}), ram pressure (Psw in nPa), IMF magnitude (Bo in nT), and Bx (nT), By (nT), and Bz (nT) components in GSM coordinate system, the SYM-H (nT) and AE (nT) indices, respectively. *The data have 1 min resolution while thin lines* in the Vsw, Nsw, and Psw panels show the 1 h average data. The *horizontal arrows* in the AE and Nsw panels indicate the HILDCAA event and the CIR interval, respectively. The *vertical line* shows the HCS.

compressed plasma density (Nsw) and IMF Bo from the start of day 259 to the middle of day 260. The CIR is followed by an HSS (peak Vsw of ~850 km s^{-1}). It is interesting to note that the HILDCAA event started with the CIR that led to only a weak geomagnetic activity for this case—the peak SYM-H during the CIR event was only −48 nT. This is not considered by Gonzalez et al. (1994) to be a magnetic storm.

Long-term moderate geomagnetic activity with peak SYM-H of −57 nT and peak AE of 2072 nT was recorded during the HSS interval. The onset of the HILDCAA event coincided with a north-to-southward turning of the IMF Bz component. The Bx and By components exhibited negative and positive polarity reversals, respectively, indicating an HCS crossing. This is denoted by a vertical line in the figure. In this case the HCS occurred in the slow-speed stream.

The top panel of Fig. 2 shows the variations of the integrated electron fluxes (in units of cm^{-2} s^{-1} sr^{-1}, hereafter called flux unit, FU) at two energy-levels: $E > 0.6$ and >2.0 MeV at geostationary orbit ($L = 6.6$). The electron fluxes were obtained from the Geostationary Operational Environmental Satellite (GOES) 8 (http://www.ngdc.noaa.gov/stp/satellite/goes/dataaccess.html) (Onsager et al., 1996). The electron fluxes are measured by the solid-state detectors with pulse height discrimination in the energetic particle sensors onboard GOES. The data were corrected for secondary responses from other sources such as >32 MeV protons, and from directions outside the nominal detector entrance apertures. The running daily averages of the high-resolution (1 min) electron fluxes were estimated to remove diurnal variations, which are well-known features of geosynchronous flux data. This effectively removes the instrument background noise level as well (e.g., Turner and Li, 2008).

The HCS crossing at ~2136 UT on day 258 (September 15) coincides with the initiation of the electron flux "dropout" (RED). The E >0.6 and >2.0 MeV electron fluxes exhibited decreases from $\sim 19 \times 10^4$ to ~13 FU, and from $\sim 23 \times 10^2$ to ~5 FU, respectively. The decreases took ~9.9 h and 8.2 h, respectively. The flux dropouts are time-coincident with the onset of an interplanetary high-density plasma feature. The plasma density Nsw increased from ~14 cm^{-3} at 2127 UT to the peak value of ~37 cm^{-3} at 2230 UT on day 258 (September 15). It decreased to ~9 cm^{-3} at 0240 UT on day 259 (September 16). The pressure pulse (Psw) started to rise at 2129 UT from a value of ~5 nPa until 2230 UT on day 258 when it reached the peak of ~10 nPa. The Psw slowly decreased to ~3 nPa at 0235 UT on day 259. It may be mentioned that Tsurutani et al. (2016) studied eight HPS pressure pulse events that were not followed by geomagnetic storms from solar cycle (SC) 23, and it was shown that all of them were associated with RED events.

Electron fluxes started to increase around the middle of day 260 (September 17) near the end of the CIR. The $E > 0.6$ and >2.0 MeV electron flux increases had time lags of >1 day and ~1.5 days, respectively, from the HILDCAA onset time. The entire HILDCAA interval thereafter was associated with enhanced fluxes of relativistic electrons.

An example of whistler-mode chorus wave generation during 1800–2100 UT on September 16, 2003, is shown in Fig. 3. This was obtained from the Cluster-4 satellite (Santolik et al., 2014). The red and yellow traces starting at ~1830 UT at ~4 kHz and descending to ~400 Hz by ~1945 UT are the chorus waves. The decrease in frequency was caused by the spacecraft moving to lower magnetic field strengths (chorus occurs from ~0.25 to ~0.75 the local equatorial electron cyclotron frequency: Tsurutani and Smith, 1974). These are marked by a red rectangle in the figure. The L value, expanding from 4.6 to ~13, corresponds to the entire outer zone magnetosphere between the nominal location of the plasmasphere to the magnetopause. The magnetic local time (MLT) for this

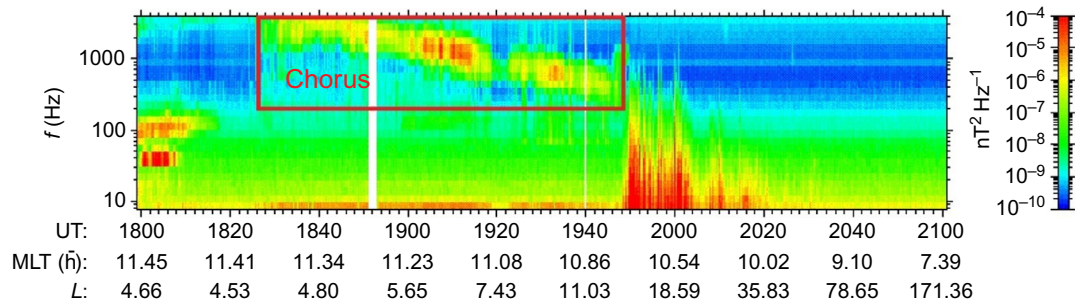

FIG. 3

The magnetic field spectrum measured by the Cluster-4 spacecraft on September 16, 2003, during the 1800–2100 UT period. The region marked by a *red rectangle* shows chorus signals.

Modified from Hajra, R., Tsurutani, B.T., Echer, E., Gonzalez, W.D., Santolik, O., 2015b. Relativistic ($E>0.6$, >2.0, and >4.0 MeV) electron acceleration at geosynchronous orbit during high-intensity, long-duration, continuous ae activity (HILDCAA) events. Astrophys. J. 799, 39, doi: 10.1088/0004-637X/799/1/39.

interval varied from 11.4 to 10.5, a region where chorus is particularly intense. Hajra et al. (2015b) analysed Cluster-4 data in the $5<L<10$, $00<\text{MLT}<6$, and $6<\text{MLT}<12$ regions during 16 HILDCAA events occurring between 2001 and 2008. All of these 16 events were found to be associated with chorus waves in both local time sectors.

Hajra et al. (2015b) identified 35 HILDCAA events during SC 23 that had good quality solar wind/interplanetary and GOES 8 and 12 relativistic electron data available for a statistical study. It was observed that the peak fluxes of $E>0.6$, >2.0, and >4.0 MeV electrons during HILDCAA intervals were always greater than those before HILDCAA initiation. The conclusion of Hajra et al. (2015b) was that HILDCAA events are always associated with flux enhancements of magnetospheric relativistic electrons.

4 SOLAR CYCLE PHASE DEPENDENCE OF ELECTRON ACCELERATION

To identify any possible dependence of relativistic electron acceleration at geostationary orbit ($L=6.6$) on SC phases, Hajra et al. (2014c) conducted a statistical study of 38 HILDCAA events during SC 23 (1995–2008). The events were sorted into different SC phases, namely, the ascending phase, solar maximum, descending phase, and solar minimum. The 11 events occurring during the ascending and solar maximum were combined and called the AMAX events. The remaining 27 events that occurred during the descending phase and solar minimum were combined and called the DMIN events.

Fig. 4 shows the superposed solar wind/interplanetary (Vsw, Nsw, IMF Bo, and Bz), geomagnetic parameters (Dst and AE) along with the fluxes of $E>2$ MeV electrons during the HILDCAA intervals. The DMIN events are shown in red, and the AMAX events are shown in blue. The reference time ($t=0$) for the superposed epoch analysis is the time of HILDCAA onset. The typical CIR signatures as discussed in Figs. 1 and 2, that is, compressions in plasma and magnetic fields at the interface between the HSS and slow stream in the antisolar direction (upstream) of the HSS, may be noted. The HILDCAA

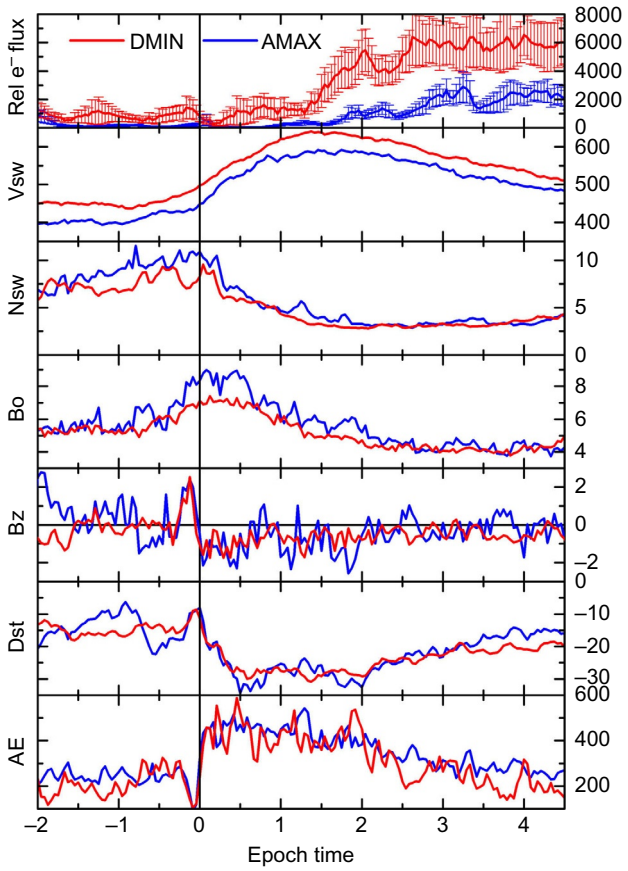

FIG. 4

Superposed time series of the relativistic electron fluxes (FU) from GOES, the solar wind speed (Vsw in km s^{-1}), the density (Nsw in cm^{-3}), the IMF magnitude (Bo in nT), the north-south component of the IMF (Bz in nT), the Dst (nT), and the AE (nT) indices during HILDCAA events. The HILDCAA onset time is taken as the zero epoch time *(vertical line)*. The time axis is in the unit of day. HILDCAA events occurring during DMIN phases and AMAX phases are shown by the *red and blue lines*, respectively.

event is found to start at the positive gradients of Vsw. This time clearly marks the sharp southward turning of the IMF Bz. The superposed HILDCAA events remarkably ordered the various interplanetary parameters.

From Fig. 4 it is clear that the solar wind/interplanetary parameters (Vsw, Nsw, IMF Bo, and Bz) exhibited more or less similar trends during both phases of the solar cycle. The Bo showed some systematic differences between the DMIN and AMAX phases, although the differences were less than the $1-\sigma$ levels. However, some significant differences were noted in the variation of Vsw. The peak HSS speed was higher for the DMIN events ($\sim$650 km s^{-1}) than for the AMAX events ($\sim$590 km s^{-1}). The HSSs also persisted for longer time in the DMIN phase than in the AMAX phase on average.

The Dst and AE indices are found to be likewise well ordered by the HILDCAA intervals during the DMIN and AMAX phase events. On the contrary, significant differences were noted in the variations of the relativistic electrons between the two phases. For the DMIN events, the flux decreased from the average initial flux level of >1000 FU to the lowest value of ~250 FU, ~4 h after the HILDCAA onset. The flux recovered to the preevent value within ~10 h of the dropout. For the AMAX events, the flux decreased from the average initial level of ~800 FU to the lowest value of ~32 FU at $t \sim 15$ h. It took longer (>1 day) than for the DMIN events to recover to the preevent flux value. The relativistic electron fluxes for both DMIN and AMAX phases start to increase at ~1.5 days after the HILDCAA onset. A maximum flux of ~6400 FU was recorded during the DMIN events. It is ~5 times the value of preevent fluxes. The maximum enhanced flux for the AMAX events was ~2900 FU, ~3.5 times the corresponding preevent value. The AMAX event peak flux was less than 50% of that during the DMIN events. During the HILDCAA intervals, the mean fluxes in the DMIN and AMAX phases were outside the $1-\sigma$ levels of one another. This implies that there may be statistically different values in the two phases.

Slightly higher and longer-lasting HSS during the DMIN phase than during the AMAX phase seems to be insignificant with respect to large flux differences between the phases. Higher solar wind speeds during the DMIN phases are expected to lead to higher solar wind electric fields and polar cap potentials. However, no such polar cap potential or electric field relative enhancements were noted in the analyses. Moreover, no other solar wind or magnetospheric parameter displayed any major difference between the solar cycle phases. To explain the solar cycle phase dependence of the relativistic electrons, Hajra et al. (2014c) proposed two possible explanations: either the relativistic electron loss rates are higher during the rising and maximum phases or the acceleration process is more efficient during the declining and minimum phases. Both the acceleration and loss of the electrons are known to be associated with the chorus (Horne and Thorne, 1998; Summers et al., 1998, 2004; Roth et al., 1999; Nakamura et al., 2000; Lorentzen et al., 2001; Meredith et al., 2002, 2003; Horne et al., 2003a, 2005a; Thorne et al., 2005; Tsurutani et al., 2006, 2013; Kasahara et al., 2009). Higher solar irradiance during solar maximum populates the dayside magnetosphere with higher thermal plasma densities (Jentsch, 1976). These higher plasma densities could act to reduce local wave phase speeds and enhance particle pitch angle scattering (Tsurutani and Smith, 1977), thus reducing the "seed" population of 10–100 keV electrons for relativistic electron growth. Another possibility is that the higher thermal plasma densities during solar maximum lead to the higher ratio of the electron plasma frequency to the electron gyrofrequency ω_{pe}/Ω_e. This might reduce the amount of acceleration, because the electron acceleration by whistler-mode waves is more efficient for the smaller ω_{pe}/Ω_e ratio (Summers et al., 1998; Horne et al., 2003b). It is possible that both mechanisms are contributing to the greater relativistic electron acceleration during the DMIN phase.

5 MAXIMUM ENERGY-LEVEL DEPENDENCE OF ELECTRON ACCELERATION

Hajra et al. (2015b) conducted a statistical analysis on the relativistic electrons at $L = 6.6$ with $E > 0.6$, >2.0, and >4.0 MeV to study the maximum energy-level dependence of the electron acceleration. Fig. 5 shows the superposed variations of the integrated electron fluxes for the SC 23 HILDCAA events. The Dst and AE panels are shown for reference. The HILDCAA onset time was taken as the zero epoch time of the superposed epoch analyses as before. The bold curves show the superposed mean values, and gray error bars show the standard $(1-\sigma)$ deviations.

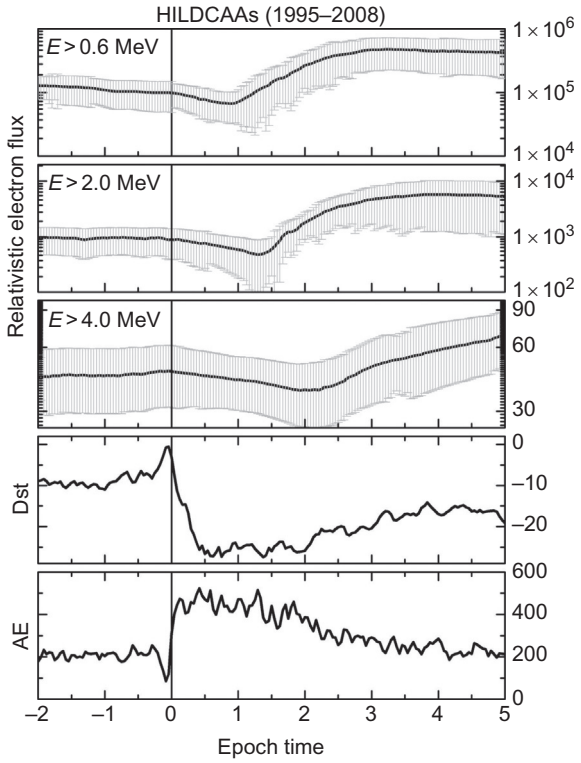

FIG. 5

Superposed time series of relativistic electron fluxes (FU) from GOES, Dst (nT), and AE (nT) indices. The energy-levels of the electrons are given in the electron panels. *Bold curves* show the mean values, and the error bars show the standard ($1-\sigma$) deviations. The zero epoch time corresponds to the initiation of HILDCAAs as in Fig. 4. The time axis is in the unit of day.

The HILDCAA interval is characterized by enhanced fluxes, and the flux enhancement is time-delayed from the HILDCAA onset. The enhancement of $E > 0.6$ MeV electrons first started $\sim$1.0 day after the statistical onset of HILDCAAs. The enhancements of $E > 2.0$ and >4.0 MeV electrons occurred $\sim$1.5 days and $\sim$2.5 days after HILDCAA onset, respectively. Higher energy electrons took longer to respond to the HILDCAA events. After the start of flux enhancement, $E > 0.6$ MeV electrons took $\sim$2.3 days to reach the maximum level of 4.8×10^5 FU, $E > 2.0$ MeV electrons took $\sim$2.4 days to reach the maximum level of 5.8×10^3 FU, and $E > 4.0$ MeV electrons reached the maximum flux level of $\sim 7.2 \times 10^1$ FU after $\sim$3.3 days. That is, acceleration timescales are longer for the higher energy electrons. The acceleration rates were $\sim 1.8 \times 10^5$, 2.2×10^3, and 1.0×10^1 FU day^{-1} for $E > 0.6$, >2.0, and >4.0 MeV electrons, respectively.

The estimated acceleration timescales are consistent with theoretical timescales of electron flux enhancement by whistler-mode chorus wave acceleration (e.g., Horne et al., 2003a). The delayed

enhancement of higher energy electrons is a characteristic feature of the wave acceleration. It is proposed that the relativistic electrons are bootstrapped from high-energy (~100 keV) electrons. The $E > 0.6$ MeV electrons are accelerated by chorus from HILDCAA-injected $E \sim 10$–100 keV electrons, the $E > 2.0$ MeV electrons are accelerated from the $E > 0.6$ MeV electron population, and consequently the $E > 4.0$ MeV electrons are accelerated from the $E > 2.0$ MeV population. The enhancements of the energetic electron population followed by higher energy relativistic electron enhancements are also reported by other works as well (Baker et al., 1979, 1998; Li et al., 2005; Turner and Li, 2008; Boyd et al., 2014, 2016; Reeves et al., 2016).

After reaching their peak flux levels, the $E > 0.6$, >2.0, and >4.0 MeV electron fluxes decayed at the rates of $\sim 0.5 \times 10^5$, 0.9×10^3, and 0.6×10^1 FU day^{-1}, respectively. The decay rates are slower than the acceleration rates. From these latter values, we estimated the probable average decay timescales of ~7.7, ~5.5, and ~4.0 days for $E > 0.6$, >2.0, and >4.0 MeV electrons, respectively. These are the times taken to reach the preevent flux level from the peak flux. The decay timescales are found to be consistent with previously reported values (see Baker et al., 2004; Goldstein et al., 2005; Meredith et al., 2006 for post magnetic storm intervals).

The plausible mechanisms for the relativistic electron losses are cyclotron resonant interactions with EMIC waves (Thorne and Kennel, 1971; Horne and Thorne, 1998; Summers et al., 1998; Meredith et al., 2006; Tsurutani et al., 2016), diamagnetic influence of the partial ring current (Kim and Chan, 1997; Ukhorskiy et al., 2006), and magnetopause shadowing (West et al., 1981; Li et al., 1997; Desorgher et al., 2000; Lyons et al., 2005; Bortnik et al. 2006; Kim et al., 2008; Ohtani et al., 2009; Hietala et al., 2014; Hudson et al., 2014). EMIC waves are reported to lead to faster MeV electron losses compared to those due to chorus and hiss (e.g., Summers et al., 2007; Tsurutani et al., 2016). EMIC waves are shown to play an important role for >1 MeV electron losses, particularly at high L values ($L \geq 5$) (Albert, 2003; Meredith et al., 2006; Summers et al., 2007; Tsurutani et al., 2016).

Resonant interaction of relativistic electrons with chorus leading to pitch angle scattering and loss to the atmosphere as "microbursts" has been proposed by many authors (Abel and Thorne, 1998; Nakamura et al., 2000; Lorentzen et al., 2001; Horne and Thorne, 2003; Summers et al., 2005; Thorne et al., 2005). However, recently Tsurutani et al. (2013) have shown that typical ~10–100 keV ionospheric microbursts with ~0.3 s durations were associated with pitch angle scattering of the electrons in the equatorial plane where the chorus subelements are coherent. The electron interaction with coherent waves leads to a "pitch angle transport" (Tsurutani et al., 2009, 2011; Lakhina et al., 2010; Bellan, 2013) which is ~3 orders of magnitude faster than that with incoherent waves as theoretically modeled by Kennel and Petschek (1966) and Tsurutani and Lakhina (1997). The problem with chorus interactions with relativistic electrons is that the interactions would have to take place away from the magnetic equator such that the local electron cyclotron frequency is considerably higher (than at the equator). Tsurutani et al. (2011) showed that off-axis chorus was only quasicoherent. Thus the cyclotron resonant interaction between relativistic electrons and quasicoherent chorus will not produce pitch angle diffusion fast enough to produce relativistic microbursts with timescales of ~0.3 s (Tsurutani et al., 2013). The authors did leave open the possibility that if there were ducts guiding the chorus so that the waves remained coherent as they propagated outward away from the magnetic equator, relativistic microbursts would be possible. However, to the authors' knowledge relativistic microbursts have not been detected in the ionosphere to date.

6 HILDCAA DURATION DEPENDENCE OF ELECTRON ACCELERATION

During SC 23, the duration (D) of the HILDCAAs varied between ~2 and 5 days, with an average duration of ~2.9 days for all HILDCAAs. The events were separated into two groups: the short-duration HILDCAAs with $D \leq 3$ days and the longer-duration HILDCAAs with $D > 3$ days. Fig. 6 shows the comparison of electron flux enhancements at $L = 6.6$ during short-duration (black curves) and longer-duration (gray curves) HILDCAA events. Flux enhancements (with respect to preevent fluxes) are always larger during the longer-duration events compared to those during the short-duration ones. At the $E > 0.6$ MeV energy-level, the flux enhancements during the short- and long-duration events are ~250% and 290%, respectively. The same for the $E > 2.0$ MeV electrons are ~400% and 520%, respectively. The $E > 4.0$ MeV electron flux enhancements during the short- and long-duration events are ~27% and 82%, respectively. During the short events, the $E > 0.6$ and >2.0 MeV electrons reached slightly higher peak fluxes compared to the longer-duration ones and started to decrease after t ~3.0 and 4.0 days, respectively. During longer-duration HILDCAAs, the $E > 0.6$ and >2.0 MeV fluxes appeared to saturate around the peak values.

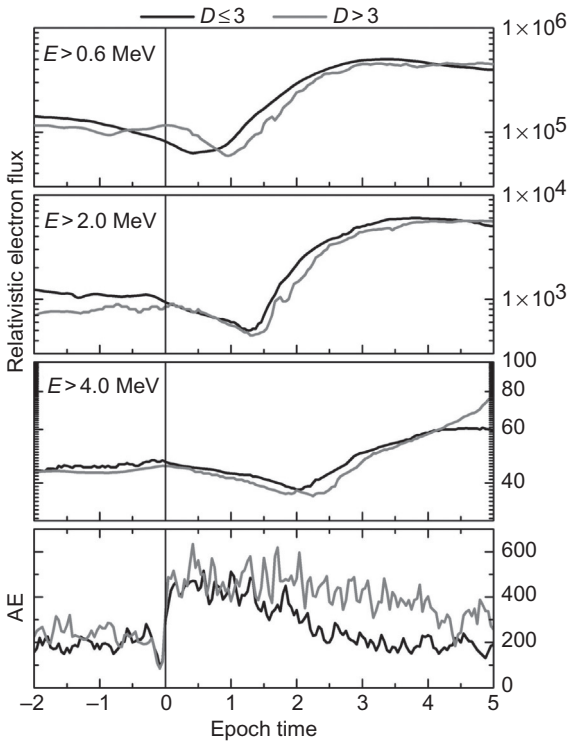

FIG. 6

Superposed time series of relativistic electron fluxes (FU) from GOES and AE (nT) index. HILDCAAs with durations $D \leq 3$ days and $D > 3$ days are shown by *black and gray curves*, respectively. The time axis is in the unit of day.

The maximum energy-level dependence on the HILDCAA duration is explained as follows. As discussed above, the intense substorm/convection events comprising the HILDCAA intervals are associated with injections of anisotropic ~10–100 keV electrons into the magnetosphere. These electrons are a source for the generation of chorus and the acceleration to even higher MeV energies. After the short-duration HILDCAAs end at ~3.0 days, the relativistic electrons undergo various loss processes, and the fluxes decay gradually. On the other hand, ~10–100 keV electrons are sporadically but continuously injected into the magnetosphere during the longer-duration HILDCAAs for longer time intervals. The electrons are accelerated to >0.6 MeV and consequently to higher ($E > 2.0$ and >4.0 MeV) energies, as proposed above. Different loss processes may occur simultaneously with the acceleration. The possible saturation-like effect observed in $E > 0.6$ MeV and $E > 2.0$ MeV electrons during the longer-HILDCAAs may be owing to a balance between acceleration and loss processes. The way to better understand the limits to this acceleration process is to make observations during extremely long HILDCAA intervals. Tsurutani et al. (1995) reported some events with ~12–25 day durations during 1973–75. It would be interesting to re-examine such older data or, better yet, see if events of this type occur during the modern Van Allen Probe epoch.

7 ARE CIR STORMS IMPORTANT?

Hajra et al. (2015a) studied the dependence of relativistic electron acceleration during HILDCAAs on the preceding geomagnetic storm main phase induced by CIRs. The HILDCAA events occurring during SC 23 were separated into: (1) events preceded by CIR-induced geomagnetic storms (SH-events) and (2) nonstorm/isolated events (H-events). The numbers of the SH- and H-events analysed in this case are 11 and 32, respectively.

Fig. 7 shows the superposed $E > 2.0$ MeV electron fluxes at $L = 6.6$, IMF Bz, Esw, SYM-H, and AE indices separately during the SH- and H-events (black and gray curves, respectively). The HILDCAA onset time was taken as the zero epoch time ($t = 0$) as before. The superposed geomagnetic indices (SYM-H and AE) display significantly different features before the HILDCAA onset and little differences during the HILDCAA interval between the SH- and H-events. The geomagnetic activity (SYM-H and AE indices) was enhanced before the SH-onset (zero epoch time) owing to the preceding geomagnetic storm main phases. A signature of the end of storm main phase ~6 h prior to the HILDCAA onset may be noted in the SYM-H variation. On the other hand, during the H-events, the SYM-H and AE indices indicate weak enhancements of ring current and auroral activity only during the HILDCAA interval. The latter interval occurred after geomagnetic calm (Tsurutani et al., 1995). The second panel of Fig. 7 shows the variation of IMF Bz. A small but significant southward Bz component may be noted before the SH onset time. This is responsible for the storm main phase. In the case of the H-events, Bz varied around 0 nT, consistent with the geomagnetic calm before event initiation. Interestingly, the initiation of the H-events was preceded by (~3 h) a prominent northward-to-southward turning of Bz. The Esw follows the variation of the IMF Bz.

The top panel of Fig. 7 shows the variation of the $E > 2.0$ MeV electron fluxes. There is no significant difference in electron fluxes between the SH- and H-events. In both cases, flux enhancements are noted to occur with time lags of ~1 day after the HILDCAA onset. The $E > 0.6$ and $E > 4.0$ MeV electron fluxes for the SH- and H-events are also similar to each other (not shown).

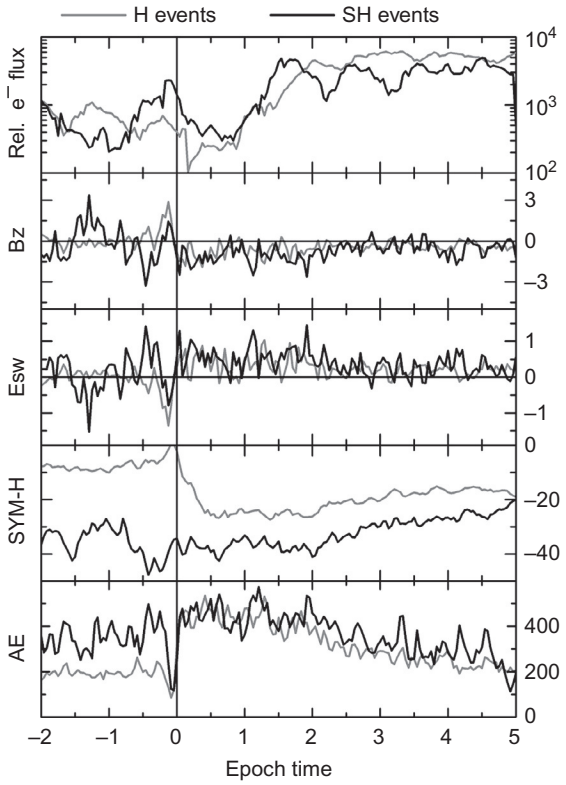

FIG. 7

Superposed time series of $E > 2.0$ MeV electron fluxes ($cm^{-2}\,s^{-1}\,sr^{-1}$), the IMF Bz (nT), Esw ($mV\,m^{-1}$), SYM-H (nT), and AE (nT) indices during HILDCAA events. The *gray and black curves* correspond to isolated HILDCAAs (H) and CIR storm-preceded HILDCAAs (SH), respectively. The time axis is in the unit of day.

Chorus generation is reported during geomagnetic storms (Horne and Thorne, 1998; Summers et al., 1998, 2002; Meredith et al., 2002; Horne et al., 2003a, 2005a,b, 2007). However, the particle injections during storms are deeper into the magnetosphere (stronger convection electric fields) and last for only hours. On the other hand, HSS/HILDCAAs can last for days to weeks (Tsurutani et al., 1995; Hajra et al., 2013), and presumably, the chorus lasts that long as well. The ~10–100 keV electron injection during HILDCAAs is somewhat shallow, involving only the outer portion of the magnetosphere, $L \sim 5$–10 (see Soraas et al., 2003) due to the relatively small convection electric fields (Tsurutani et al., 2006). Thus it is surmised that the electron acceleration is taking place at L values close to geosynchronous orbit. The NOAA GOES satellites might be in ideal locations to monitor events of this type. It may be mentioned that the results presented in the present review paper are based on observations by geostationary GOES satellites placed at the Earth's outer radiation belt ($L = 6.6$). Further study can be performed using measurements by Van Allen Probes that cover a wide range of L values to verify this hypothesis.

8 RELATIVISTIC ELECTRON VARIATION DURING ICME MAGNETIC STORMS

Relativistic electron losses have been noted in times during and around ICME-induced geomagnetic storms (e.g., Baker et al., 1994; Onsager et al., 2002; Reeves et al., 2003; Horne et al., 2009; Kim et al., 2010, 2011; Turner et al., 2013, 2014; Hietala et al., 2014; Hudson et al., 2014). A number of different processes have been identified: losses due to gradient drift in compressed magnetic fields such as due to shocks (Li et al., 1997; Desorgher et al., 2000; Lyons et al., 2005; Kim et al., 2008, 2010; Ohtani et al., 2009), losses due to magnetospheric inflation by the enhanced ring current (Kim and Chan, 1997; Ukhorskiy et al., 2006; Bortnik et al., 2006; Kim et al., 2010), and losses due to radial diffusion (Kellogg, 1959; Vernov et al., 1960; Fei et al., 2006; Shprits et al., 2006; Kim et al., 2011; Hietala et al., 2014). These processes are known as "magnetopause shadowing" that lead to particle losses at the magnetopause (Dessler and Karplus, 1961; West et al. 1972; Li et al., 1997; Desorgher et al., 2000; Lyons et al., 2005; Kim et al., 2008; Ohtani et al., 2009; Albert, 2014; Hietala et al., 2014; Hudson et al., 2014; Roederer and Zhang, 2014). There are also particle losses due to magnetic erosion or magnetic reconnection (Baker et al., 2013; Hudson et al., 2014; Ni et al., 2016). These latter particles are lost down tail. And finally, wave-particle interactions will lead to particle losses into the ionosphere (Thorne and Kennel, 1971; Meredith et al., 2003; Summers and Thorne, 2003; Thorne et al., 2005; Summers et al., 2007; Usanova et al., 2014; Tsurutani et al., 2016).

Particle acceleration during geomagnetic storms can be accomplished in several different ways. Particles can be energized by nightside storm time convection electric fields (Li et al., 2003; Hori et al., 2005; Xie et al., 2006; Wygant et al., 2013). PC5 oscillations can lead to radial diffusion (Schulz and Lanzerotti, 1974; Hudson et al., 2000). The electrons can be energized by substorm injection during the storms (e.g., Baker et al., 1998, 2014; Miyoshi et al., 2013; Thorne et al., 2013; Foster et al., 2014; Jaynes et al., 2015). Chorus generated during the storms and substorms can accelerate the electrons (Horne and Thorne, 1998; Summers et al., 1998; Roth et al., 1999; Meredith et al., 2003; Thorne et al., 2013). Other waves have been mentioned for electron acceleration as well (Selesnick and Blake, 2000; Meredith et al., 2002; Summers et al., 2002; Miyoshi et al., 2003; Horne et al., 2007; Thorne et al., 2013; Tsurutani et al., 2013; Boyd et al., 2014).

Fig. 8 shows an example of a geomagnetic storm that occurred during March 17–21, 2015. This is the biggest magnetic storm of SC 24 with peak SYM-H intensity of −234 nT. The associated interplanetary phenomena are characterized by an interplanetary shock and a magnetic cloud (MC) followed by a HSS.

8.1 FAST SHOCK, SHEATH, AND FIRST MAGNETIC STORM

The fast-forward shock at 0448 UT on March 17 (marked by the vertical dotted line in the figure) is identified by a jump in Vsw from ∼397 to 518 km s^{-1} (Fig. 8D), in Nsw from ∼11 to 36 cm^{-3} (Fig. 8E), in Psw from ∼4 to 19 nPa (Fig. 8E) and in IMF Bo from ∼8 to 28 nT (Fig. 8G). The shock is related to the C9-class solar flare erupted by the sunspot AR2297 on March 16. Higher resolution (3 s) interplanetary data from the WIND spacecraft (http://wind.gsfc.nasa.gov/mfi_swe_plot.php) were used to perform interplanetary shock analyses. The shock normal direction is calculated using the Abraham-Schrauner (1972) method, and then the Rankine-Hugoniot conservation equations are used to get the shock speed (Smith, 1985; Tsurutani and Lin, 1985; Tsurutani et al., 2011). The shock was found to have a magnetosonic Mach number of 2.9 and a shock normal angle of 63 degrees relative

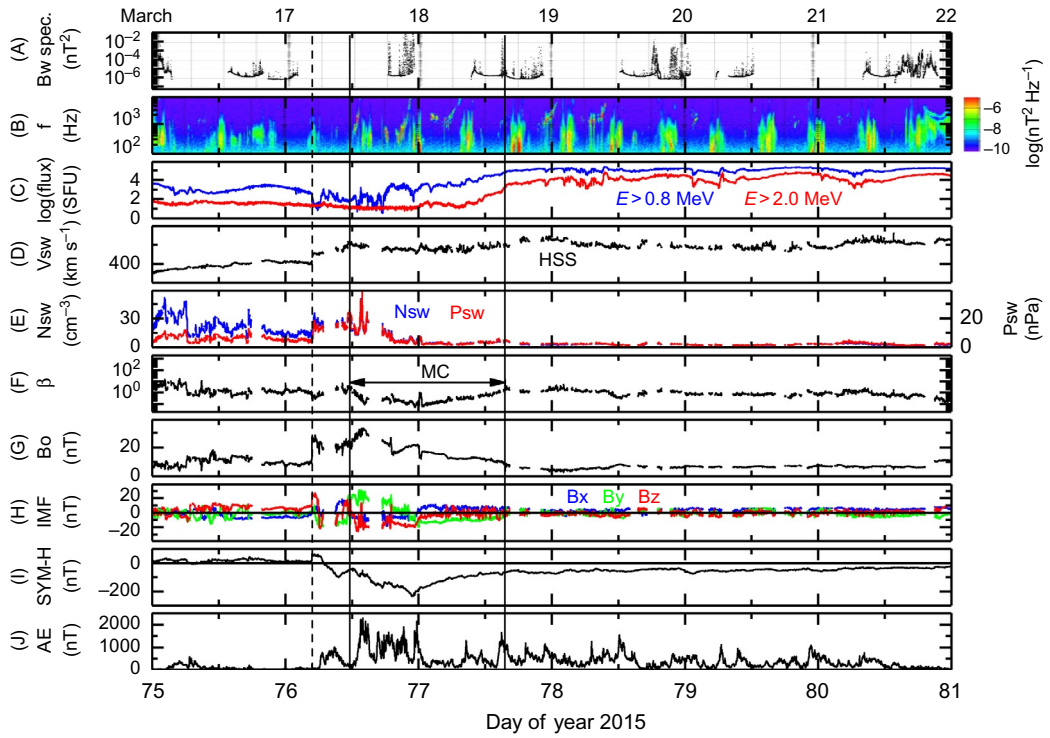

FIG. 8

Geomagnetic storm occurring on March 17–21, 2015. From top to bottom, the panels show the variations of (A) the lower-band chorus wave amplitudes integrated over 0.1–0.5fce measured by the EMFISIS instrument on VAP-A and VAP-B, (B) the frequency-time spectrogram of wave magnetic field spectral density in the WFR channel observed by VAP-A, (C) $E>0.8$ *(blue)* and $E>2.0$ MeV *(red)* electron fluxes measured by GOES-15, (D) solar wind speed Vsw, (E) plasma density Nsw (*blue*, scale on the left) and ram pressure Psw (*red*, scale on the right), (F) plasma β, (G) IMF magnitude Bo, (H) Bx *(blue)*, By *(green)*, and Bz *(red)* components of IMF in GSM coordinate system, (I) the SYM-H, and (J) AE indices, respectively. The *vertical dotted line* indicates an interplanetary fast-forward shock. The region between the *dotted line* and the first *solid line* is the sheath interval. This is followed by an MC, the region between the two *solid lines*. This is also marked by a *horizontal arrow* in the plasma β panel. An HSS follows the MC.

to the upstream magnetic field. The shock and the high plasma density sunward of it caused a sudden impulse (SI^+) in SYM-H of ~+67 nT (Fig. 8I). The shock triggered a nightside substorm with a peak AE of ~1016 nT at 0852 UT (Fig. 8J). This is the storm initial phase where the high ram pressure behind the interplanetary shock compressed the magnetosphere.

Immediately after the shock is a magnetic sheath continuing until ~1136 UT on March 17. The sheath is characterized by multiple IMF Bz changes with a peak value of ~−22 nT (Fig. 8H), high plasma density Nsw ~30 cm^{-3} (Fig. 8E), and high plasma β ~7 (Fig. 8F). This is followed by an MC, from ~1136 UT on March 17 to ~1533 UT on March 18 (marked by a horizontal arrow in

the plasma β panel). The MC is identified by the low plasma β ~0.05 (Fig. 8F), positive-negative rotation in Bx and negative-positive rotation in By (Fig. 8H). The IMF Bz turns southward from northward polarity during this interval (Fig. 8H). The MC had a peak southward IMF of ~−26 nT.

The first storm main phase started at ~0550 UT on March 17 following the interplanetary shock. SYM-H reached a local minimum of −101 nT at ~0937 UT. This storm main phase is caused by sheath southward IMF fields (peak ~−22 nT) immediately after the shock.

8.2 MAGNETIC CLOUD (MC) AND SECOND AND THIRD STORMS

Fig. 8I shows second storm main phase occurred with a deeper minimum of SYM-H = − 177 nT at ~1728 UT. The third storm main phase with peak value of SYM-H = − 234 nT was reached at ~2247 UT on March 17. Both storms are caused by southward IMFs within an MC. The second and third storm main phases correspond to peak IMF southward fields of ~−26 nT and −20 nT at ~1307 UT and 2153 UT on March 17, respectively.

The three storm main phases had a total duration of ~17 h. The peak AE intensity was ~2300 nT and occurred near the beginning of the second storm main phase. The final recovery phase of the storm starts with a northward turning of the IMF Bz to ~0 nT at ~2247 UT on March 17. It is believed that this is still part of the MC because of the low plasma β.

8.3 HSS AND STORM RECOVERY PHASE

The storm "recovery" corresponds to the HSS interval (Fig. 8D) following the MC. A long-duration and slow "recovery" in the SYM-H index is apparent in the figure from 2247 UT on March 17 to ~0033 UT on March 23. The "recovery phase" is characterized by a HILDCAA event.

An HSS follows immediately after the MC and extends from the end of the cloud at ~1533 UT on March 18 until the end of the interval shown (Fig. 8D). This is consistent with the detection of a solar coronal hole during March 15–19. The HSS had a peak speed of ~690 km s^{-1} at ~2301 UT on March 18. The magnetic field intensity was ~33 nT. The HSS carried Alfvén waves characterized by northward-southward fluctuations in IMF Bz with peak southward component of ~−7 nT.

The magnetic storm "recovery" is ~5 days, much longer than the typical ~10 h for the decay time scale of ring current particles by charge exchange, Coulomb collisions, wave-particle interactions, and plasma convection out of the dayside magnetopause (e.g., Kozyra et al., 1998). The southward component of the Alfvén waves leads to short bursts of magnetic reconnection (Tsurutani et al., 1995) causing the injection of plasma into the midnight sector of the magnetosphere, leading to a near steady state of the ring current energy (Soraas et al., 2003).

8.4 RELATIVISTIC ELECTRON FLUX VARIABILITY DURING THE COMPLEX INTERPLANETARY EVENT: SHOCK EFFECTS

Fig. 8C shows relativistic $E > 0.8$ and > 2.0 MeV electrons measured by GOES 15 at $L = 6.6$. The $E > 0.8$ MeV electron fluxes decrease by ~2 orders of magnitude and the $E > 2.0$ MeV electrons by ~1 order of magnitude during the main phase. The decrease in the $E > 0.8$ MeV electrons is quite abrupt and coincident with occurrence of the shock (shown by a vertical dotted line).

8.5 ELECTRON ACCELERATION

During the storm recovery phase, which is accompanied by the HSS, the relativistic electron fluxes are noted to be larger than the storm main phase as well as than the prestorm period (i.e., there is an overall flux enhancement). The increase is by ~4 orders of magnitude.

The wave activity during the geomagnetic storm was observed by NASA's twin Van Allen Probes: VAP-A and VAP-B (http://vanallenprobes.jhuapl.edu/index.php) (Mauk et al., 2012). Fig. 8A shows the lower-band chorus waves observed by the Electric and Magnetic Field Instrument Suit and Integrated Science (EMFISIS) (Kletzing et al., 2013; Wygant et al., 2013). The chorus wave amplitudes were calculated by integrating the magnetic wave power spectral density over 0.1–0.5 fce, where fce is the electron cyclotron frequency. The wave power spectral density obtained from the waveform receiver (WFR) on the EMFISIS instrument (Kletzing et al., 2013) is shown in Fig. 8B. Enhanced whistler-mode wave (hiss and chorus) activities may be noted during the geomagnetic storm recovery phase (Fig. 8B). The waves had the peak spectral density of $\sim 10^{-3}$ nT^2 Hz^{-1}. The waves are seen in all passes of the VAPs, indicating possibly continuous wave activity throughout the recovery phase.

9 CONCLUSIONS

The outer radiation belt relativistic electron variation is of physical interest in understanding the radiation belt dynamics and space weather in general. Also, these have practical importance for hazardous effects to orbiting spacecraft. These are known as "killer electrons" that can cause outages and failures of satellite electronics (Baker et al., 1994, 2004; Wrenn, 1995; Blake et al., 1997; Horne, 2003). The works by Hajra et al. (2013, 2014c, 2015a,b) and Tsurutani et al. (2016), reviewed above, clearly present the outer radiation belt relativistic electron variation as a cyclical process controlled by interplanetary phenomena.

The declining phase of the solar cycle is the most important period for large-scale variability in the relativistic electron loss and acceleration processes. Interplanetary space is dominated by HSSs during this phase. The interplanetary HPS impinging on the magnetosphere leads to the loss of the relativistic electrons through the interactions with EMIC waves and magnetopause shadowing. The HPS occurs in the slow solar wind followed by the CIR and HSS. The HSS, which carries the interplanetary Alfvén waves, causes substorms and convection events and energetic ~10–100 keV electron injections into the nightside sector of the magnetosphere. The electrons are accelerated to relativistic energies through resonant interactions with electromagnetic plasma waves called chorus.

The magnetic reconnection between the geomagnetic field and the southward component of the Alfvén waves results in intense auroral activity known as HILDCAA events. The HILDCAAs occurring in the geomagnetic storm recovery phase or in geomagnetic moderately quiet conditions are shown to be associated with magnetospheric electron acceleration to relativistic energies. Most interestingly, the electron acceleration starts ~1 day or more after the HILDCAA onset. This indicates the probability that magnetospheric relativistic electron acceleration may be predicted more than 1 day in advance using ground-based observations of auroral activity (HILDCAAs) during HSSs. Prediction models of geomagnetic indices based on solar wind parameters may be utilized for this purpose (e.g., Temerin and Li, 2006; Li et al., 2007; Luo et al., 2013).

Hajra et al. (2015b) noted that the acceleration of $E > 4.0$ MeV electrons is delayed from the acceleration of $E > 2.0$ MeV electrons and thus a "bootstrap" process was in effect. It will be interesting to find out what the upper limit of relativistic electron energy might be from the chorus-energetic electron interaction process. Tsurutani et al. (1995) noted extremely long-lasting HSSs during 1973–75, a feature that has never recurred since that epoch. Is it possible that even higher energies could be produced, and if so, what effects might that have on Earth-orbiting spacecraft?

The case study of an ICME storm shows clear evidence of relativistic electron losses by an interplanetary shock impingement. The loss process is most probably magnetopause shadowing and wave-particle interactions with EMIC waves (Tsurutani et al., 2016, and references therein). During the storm recovery, the one clear cause of relativistic electron repopulation is chorus associated with the HSS/HILDCAA event following the ICME. The flux levels in the storm recovery phase are larger than the preshock levels in this case. Other contributors to relativistic electron repopulation during magnetic storms would be (1) storm time convection electric fields, (2) substorms injections during and after the storm, and (3) chorus and other wave mode acceleration.

The reader can note some of the similarities between the ICME storm case and the low-speed high-speed solar declining phase case. For example, if it is shocks that cause the particle losses (instead of the HPS) and then injection and chorus or PC5 acceleration, then one notes a clear analogy.

REFERENCES

Abel, B., Thorne, R.M., 1998. Electron scattering loss in the Earth's inner magnetosphere: 1 Dominant physical processes. J. Geophys. Res. 103, 2385–2396. https://doi.org/10.1029/97JA02919.

Abraham-Schrauner, B., 1972. Determination of magnetohydrodynamic shock normal. J. Geophys. Res. 77, 736–739. https://doi.org/10.1029/JA077i004p00736.

Albert, J.M., 2003. Evaluation of quasi-linear diffusion coefficients for EMIC waves in a multispecies plasma. J. Geophys. Res. 108, 1249. https://doi.org/10.1029/2002JA009792.

Albert, J.M., 2014. Radiation diffusion simulations of the 20 September 2007 radiation belt dropout. Ann. Geophys. 32, 925–934. https://doi.org/10.5194/angeo-32-925-2014.

Baker, D.N., Higbie, P.R., Belian, R.D., Hones Jr., E.W., 1979. Do Jovian electrons influence the terrestrial outer radiation zone? Geophys. Res. Lett. 6, 531–534. https://doi.org/10.1029/GL006i006p00531.

Baker, D.N., Blake, J.B., Klebesadel, R.W., Higbie, P.R., 1986. Highly relativistic electrons in the Earth's outer magnetosphere: 1. Life-times and temporal history 1979–1984. J. Geophys. Res. 91, 4265–4276. https://doi.org/10.1029/JA091iA04p04265.

Baker, D.N., McPherron, R.L., Cayton, T.E., Klebesadel, R.W., 1990. Linear prediction filter analysis of relativistic electron properties at 6.6 RE. J. Geophys. Res. 95, 15133–15140.

Baker, D.N., Blake, J.B., Callis, L.B., Cummings, J.R., Hovestadt, D., Kanekal, S., Klecker, B., Mewaldt, R.A., Zwickl, R.D., 1994. Relativistic electron acceleration and decay time scales in the inner and outer radiation belts: SAMPEX. Geophys. Res. Lett. 21, 409–412.

Baker, D.N., Li, X., Blake, J.B., Kanekal, S., 1998. Strong electron acceleration in the Earth's magnetosphere. Adv. Space Res. 21, 609–613.

Baker, D.N., Kanekal, S.G., Li, X., Monk, S.P., Goldstein, J., Burch, J.L., 2004. An extreme distortion of the Van Allen belt arising from the 'Hallowe'en' solar storm in 2003. Nature 432, 878–881.

Baker, D.N., Kanekal, S.G., Hoxie, V.C., Henderson, M.G., Li, X., Spence, H.E., Elkington, S.R., Friedel, R.H.W., Goldstein, J., Hudson, M.K., Reeves, G.D., Thorne, R.M., Kletzing, C.A., Claudepierre, S.G., 2013.

A long-lived relativistic electron storage ring embedded within the Earth's outer Van Allen radiation zone. Science 340, 186–190. https://doi.org/10.1126/science.1233518.

Baker, D.N., Jaynes, A.N., Li, X., Henderson, M.G., Kanekal, S.G., Reeves, G.D., Spence, H.E., Claudepierre, S.G., Fennell, J.F., Hudson, M.K., Thorne, R.M., Foster, J.C., Erickson, P.J., Malaspina, D.M., Wygant, J.R., Boyd, A., Kletzing, C.A., Drozdov, A., Shprits, Y.Y., 2014. Gradual diffusion and punctuated phase space density enhancements of highly relativistic electrons: Van Allen Probes observations. Geophys. Res. Lett. 41, 1351–1358. https://doi.org/10.1002/2013GL058942.

Belcher, J.W., Davis Jr., L., 1971. Large-amplitude Alfvén waves in the interplanetary medium: 2. J. Geophys. Res. 76, 3534–3563. https://doi.org/10.1029/JA076i016p03534.

Bellan, P.M., 2013. Pitch angle scattering of an energetic magnetized particle by a circularly polarized electromagnetic wave. Phys. Plasmas 20. 042117. https://doi.org/10.1063/1.4801055.

Blake, J.B., Baker, D.N., Turner, N., Ogilvie, K.W., Lepping, R.P., 1997. Correlation of changes in the outer-zone relativistic electron population with upstream solar wind and magnetic field measurements. Geophys. Res. Lett. 24, 927–929.

Bortnik, J., Thorne, R.M., O'Brien, T.P., Green, J.C., Strangeway, R.J., Shprits, Y.Y., Baker, D.N., 2006. Observation of two distinct, rapid loss mechanisms during the 20 November 2003 radiation belt dropout event. J. Geophys. Res. 111. A12216. https://doi.org/10.1029/2006JA011802.

Boyd, A.J., Spence, H.E., Claudepierre, S.G., Fennell, J.F., Blake, J.B., Baker, D.N., Reeves, G.D., Turner, D.L., 2014. Quantifying the radiation belt seed population in the March 17, 2013 electron acceleration event. Geophys. Res. Lett. 41, 2275–2281. https://doi.org/10.1002/2014GL059626.

Boyd, A.J., Spence, H.E., Huang, C.L., Reeves, G.D., Baker, D.N., Turner, D.L., Claudepierre, S.G., Fennell, J.F., Blake, J.B., Shprits, Y.Y., 2016. Statistical properties of the radiation belt seed population. J. Geophys. Res. 121, 7636–7646. https://doi.org/10.1002/2016JA022652.

Brice, N., 1964. Fundamentals of very low frequency emission generation mechanisms. J. Geophys. Res. 69, 4515–4522. https://doi.org/10.1029/JZ069i021p04515.

Chakraborty, S.K., Hajra, R., Paul, A., 2008. Ionosphere near the anomaly crest in Indian zone during magnetic storm on 13–14 March 1989. Indian J. Radio Space Phys. 37, 396–407.

DeForest, S.E., McIlwain, C.E., 1971. Plasma clouds in the magnetosphere. J. Geophys. Res. 76, 3587–3611. https://doi.org/10.1029/JA076i016p03587.

Desorgher, L., Bühler, P., Zehnder, A., Flückiger, E.O., 2000. Simulation of the outer radiation belt electron flux decrease during the March 26, 1995, magnetic storm. J. Geophys. Res. 105, 21211–21223. https://doi.org/10.1029/2000JA900060.

Dessler, A.J., Karplus, R., 1961. Some effects of diamagnetic ring currents on Van Allen radiation. J. Geophys. Res. 66, 2289–2295. https://doi.org/10.1029/JZ066i008p02289.

Dragt, A.J., Austin, M.M., White, R.S., 1966. Cosmic ray and solar proton albedo neutron decay injection. J. Geophys. Res. 71, 1293–1304.

Dungey, J.W., 1961. Interplanetary magnetic field and the auroral zones. Phys. Rev. Lett. 6, 47–48.

Echer, E., Gonzalez, W.D., Tsurutani, B.T., 2008. Interplanetary conditions leading to superintense geomagnetic storms (Dst $\leq$ -250 nT) during solar cycle 23. Geophys. Res. Lett. 35. L06S03. https://doi.org/10.1029/2007GL031755.

Fei, Y., Chan, A.A., Elkington, S.R., Wiltberger, M.J., 2006. Radial diffusion and MHD particle simulations of relativistic electron transport by ULF waves in the September 1998 storm. J. Geophys. Res. 111. A12209. https://doi.org/10.1029/2005JA011211.

Fennell, J.F., Claudepierre, S.G., Blake, J.B., O'Brien, T.P., Clemmons, J.H., Baker, D.N., Spence, H.E., Reeves, G.D., 2015. Van Allen Probes show that the inner radiation zone contains no MeV electrons: ECT/MagEIS data. Geophys. Res. Lett. 42, 1283–1289. https://doi.org/10.1002/2014GL062874.

Foster, J.C., Erickson, P.J., Baker, D.N., Claudepierre, S.G., Kletzing, C.A., Kurth, W., Reeves, G.D., Thaller, S.A., Spence, H.E., Shprits, Y.Y., Wygant, J.R., 2014. Prompt energization of relativistic and highly

relativistic electrons during a substorm interval: Van Allen Probes observations. Geophys. Res. Lett. 41, 20–25. https://doi.org/10.1002/2013GL058438.

Frank, L., Van Allen, J.A., Whelpley, W.A., Craven, J.D., 1963. Absolute intensities of geomagnetically trapped particles with Explorer 14. J. Geophys. Res. 68, 1573–1579.

Freeman Jr., J.W., 1964. The morphology of the electron distribution in the outer radiation zone and near the magnetospheric boundary as observed by Explorer 12. J. Geophys. Res. 69, 1691–1723. https://doi.org/10.1029/JZ069i009p01691.

Friedel, R.H.W., Reeves, G.D., Obara, T., 2002. Relativistic electron dynamics in the inner magnetosphere—a review. J. Atmos. Sol. Terr. Phys. 64, 265–282. https://doi.org/10.1016/S1364-6826(01)00088-8.

Goldstein, J., Kanekal, S.G., Baker, D.N., Sandel, B.R., 2005. Dynamic relationship between the outer radiation belt and the plasmapause during March–May 2001. Geophys. Res. Lett. 32. L15104. https://doi.org/10.1029/2005GL023431.

Gonzalez, W.D., Mozer, F.S., 1974. A quantitative model for the potential resulting from reconnection with an arbitrary interplanetary magnetic field. J. Geophys. Res. 79, 4186–4194. https://doi.org/10.1029/JA079i028p04186.

Gonzalez, W.D., Joselyn, J.A., Kamide, Y., Kroehl, H.W., Rostoker, G., Tsurutani, B.T., Vasyliunas, V., 1994. What is a geomagnetic storm? J. Geophys. Res. 99, 5771–5792.

Gonzalez, W.D., Guarnieri, F.L., Clua-Gonzalez, A.L., Echer, E., Alves, M.V., Oginoo, T., Tsurutani, B.T., 2006. Magnetospheric energetics during HILDCAAs. In: Tsurutani, B.T. et al. (Ed.), Recurrent Magnetic Storms: Corotating Solar Wind Streams. Geophysical Monograph Series, vol. 167. AGU, Washington, DC, pp. 175–182. https://doi.org/10.1029/167GM15.

Guarnieri, F.L., 2006. The nature of auroras during high-intensity long-duration continuous AE activity (HILDCAA) events: 1998–2001. In: Tsurutani, B.T. et al. (Ed.), Recurrent Magnetic Storms: Corotating Solar Wind Streams. Geophysical Monograph Series, vol. 167. AGU, Washington, DC, pp. 235–243.

Hajra, R., 2011. A Study on the Variability of Total Electron Content Near the Crest of the Equatorial Anomaly in the Indian Zone (Ph.D. thesis). University of Calcutta, India.

Hajra, R., Chakraborty, S.K., DasGupta, A., 2010. Ionospheric effects near the magnetic equator and the anomaly crest of the Indian longitude zone during a large number of intense geomagnetic storms. J. Atmos. Sol. Terr. Phys. 72, 1299–1308.

Hajra, R., Echer, E., Tsurutani, B.T., Gonzalez, W.D., 2013. Solar cycle dependence of High-Intensity Long-Duration Continuous AE Activity (HILDCAA) events, relativistic electron predictors? J. Geophys. Res. 118, 5626–5638. https://doi.org/10.1002/jgra.50530.

Hajra, R., Echer, E., Tsurutani, B.T., Gonzalez, W.D., 2014a. Solar wind-magnetosphere energy coupling efficiency and partitioning: HILDCAAs and preceding CIR storms during solar cycle 23. J. Geophys. Res. 119, 2675–2690. https://doi.org/10.1002/2013JA019646.

Hajra, R., Echer, E., Tsurutani, B.T., Gonzalez, W.D., 2014b. Superposed epoch analyses of HILDCAAs and their interplanetary drivers: solar cycle and seasonal dependences. J. Atmos. Sol. Terr. Phys. 121, 24–31.

Hajra, R., Tsurutani, B.T., Echer, E., Gonzalez, W.D., 2014c. Relativistic electron acceleration during high-intensity, long-duration, continuous AE activity (HILDCAA) events: solar cycle phase dependences. Geophys. Res. Lett. 41, 1876–1881. https://doi.org/10.1002/2014GL059383.

Hajra, R., Tsurutani, B.T., Echer, E., Gonzalez, W.D., Brum, C.G.M., Vieira, L.E.A., Santolik, O., 2015a. Relativistic electron acceleration during HILDCAA events: are precursor CIR magnetic storms important? Earth Planets Space 67, 109. https://doi.org/10.1186/s40623-015-0280-5.

Hajra, R., Tsurutani, B.T., Echer, E., Gonzalez, W.D., Santolik, O., 2015b. Relativistic ($E > 0.6$, >2.0, and >4.0 MeV) electron acceleration at geosynchronous orbit during high-intensity, long-duration, continuous ae activity (HILDCAA) events. Astrophys. J. 799 (39). https://doi.org/10.1088/0004-637X/799/1/39.

Hajra, R., Tsurutani, B.T., Brum, C.G.M., Echer, E., 2017. High-speed solar wind stream effects on the topside ionosphere over Arecibo: a case study during solar minimum. Geophys. Res. Lett. 44, 7607–7617. https://doi.org/10.1002/2017GL073805.

Hietala, H., Kilpua, E.K.J., Turner, D.L., Angelopoulos, V., 2014. Depleting effects of ICME-driven sheath regions on the outer electron radiation belt. Geophys. Res. Lett. 41, 2258–2265. https://doi.org/10.1002/2014GL059551.

Hori, T., Lui, A.T.Y., Ohtani, S., Brandt, P.C., Mauk, B.H., McEntire, R.W., Maezawa, K., Mukai, T., Kasaba, Y., Hayakawa, H., 2005. Storm-time convection electric field in the near-Earth plasma sheet. J. Geophys. Res. 110. A04213. https://doi.org/10.1029/2004JA010449.

Horne, R.B., 2003. Rationale and requirements for a European space weather programme. In: Proceedings of ESA Workshop, ESTEC, Noordwijk, The Netherlands.

Horne, R.B., Thorne, R.M., 1998. Potential waves for relativistic electron scattering and stochastic acceleration during magnetic storms. Geophys. Res. Lett. 25, 3011–3014. https://doi.org/10.1029/98GL01002.

Horne, R.B., Thorne, R.M., 2003. Relativistic electron acceleration and precipitation during resonant interactions with whistler-mode chorus. Geophys. Res. Lett. 30, 1527. https://doi.org/10.1029/2003GL016973.

Horne, R.B., Meredith, N.P., Thorne, R.M., Heynderickx, D., Iles, R.H.A., Anderson, R.R., 2003a. Evolution of energetic electron pitch angle distributions during storm time electron acceleration to megaelectronvolt energies. J. Geophys. Res. 108, 1016. https://doi.org/10.1029/2001JA009165.

Horne, R.B., Glauert, S.A., Thorne, R.M., 2003b. Resonant diffusion of radiation belt electrons by whistler-mode chorus. Geophys. Res. Lett. 30, 1493. https://doi.org/10.1029/2003GL016963.

Horne, R.B., Thorne, R.M., Glauert, S.A., Albert, J.M., Meredith, N.P., Anderson, R.R., 2005a. Timescale for radiation belt electron acceleration by whistler mode chorus waves. J. Geophys. Res. 110. A03225. https://doi.org/10.1029/2004JA010811.

Horne, R.B., Thorne, R.M., Shprits, Y.Y., Meredith, N.P., Glauert, S.A., Smith, A.J., Kanekal, S.G., Baker, D.N., Engebretson, M.J., Posch, J.L., Spasojevic, M., Inan, U.S., Pickett, J.S., Decreau, P.M.E., 2005b. Wave acceleration of electrons in the Van Allen radiation belts. Nature 437 (7056), 227–230. https://doi.org/10.1038/nature03939.

Horne, R.B., Thorne, R.M., Glauert, S.A., Meredith, N.P., Pokhotelov, D., Santolik, O., 2007. Electron acceleration in the Van Allen radiation belts by fast magnetosonic waves. Geophys. Res. Lett. 34. L17107. https://doi.org/10.1029/2007GL030267.

Horne, R.B., Lam, M.M., Green, J.C., 2009. Energetic electron precipitation from the outer radiation belt during geomagnetic storms. Geophys. Res. Lett. 36. L19104. https://doi.org/10.1029/2009GL040236.

Hudson, M.K., Elkington, S.R., Lyon, J.G., Goodrich, C.C., 2000. Increase in relativistic electron flux in the inner magnetosphere: ULF wave mode structure. Adv. Space Res. 25, 2327–2337. https://doi.org/10.1016/S0273-1177(99)00518-9.

Hudson, M.K., Baker, D.N., Goldstein, J., Kress, B.T., Paral, J., Toffoletto, F.R., Wiltberger, M., 2014. Simulated magnetopause losses and Van Allen Probe flux dropouts. Geophys. Res. Lett. 41, 1113–1118. https://doi.org/10.1002/2014GL059222.

Inan, U.S., Bell, T.F., Helliwell, R.A., 1978. Nonlinear pitch angle scattering of energetic electrons by coherent VLF waves in the magnetosphere. J. Geophys. Res. 83, 3235–3253.

Jaynes, A.N., Baker, D.N., Singer, H.J., Rodriguez, J.V., Loto'aniu, T.M., Ali, A.F., Elkington, S.R., Li, X., Kanekal, S.G., Claudepierre, S.G., Fennell, J.F., Li, W., Thorne, R.M., Kletzing, C.A., Spence, H.E., Reeves, G.D., 2015. Source and seed populations for relativistic electrons: their roles in radiation belt changes. J. Geophys. Res. 120, 7240–7254. https://doi.org/10.1002/2015JA021234.

Jentsch, V., 1976. Electron precipitation in morning sector of the auroral zone. J. Geophys. Res. 81, 135–146.

Kasahara, Y., Miyoshi, Y., Omura, Y., Verkhoglyadova, O.P., Nagano, I., Kimura, I., Tsurutani, B.T., 2009. Simultaneous satellite observations of VLF chorus, hot and relativistic electrons in a magnetic storm "recovery" phase. Geophys. Res. Lett. 36. L01106. https://doi.org/10.1029/2008GL036454.

Kellogg, P.J., 1959. Van Allen radiation of solar origin. Nature 183, 1295–1297. https://doi.org/10.1038/1831295a0.

Kennel, C.F., Petschek, H.E., 1966. Limit on stable trapped particle fluxes. J. Geophys. Res. 71, 1–28. https://doi.org/10.1029/JZ071i001p00001.

Kilpua, E.K.J., Hietala, H., Turner, D.L., Koskinen, H.E.J., Pulkkinen, T.I., Rodriguez, J.V., Reeves, G.D., Claudepierre, S.G., Spence, H.E., 2015. Unraveling the drivers of the storm time radiation belt response. Geophys. Res. Lett. 42, 3076–3084. https://doi.org/10.1002/2015GL063542.

Kim, H.J., Chan, A.A., 1997. Fully adiabatic changes in storm time relativistic electron fluxes. J. Geophys. Res. 102, 22107–22116. https://doi.org/10.1029/97JA01814.

Kim, K.C., Lee, D.Y., Kim, H.J., Lyons, L.R., Lee, E.S., Öztürk, M.K., Choi, C.R., 2008. Numerical calculations of relativistic electron drift loss effect. J. Geophys. Res. 113. A09212. https://doi.org/10.1029/2007JA013011.

Kim, K.C., Lee, D.Y., Kim, H.J., Lee, E.S., Choi, C.R., 2010. Numerical estimates of drift loss and Dst effect for outer radiation belt relativistic electrons with arbitrary pitch angle. J. Geophys. Res. 115. A03208. https://doi.org/10.1029/2009JA014523.

Kim, K.C., Lee, D.Y., Shprits, Y., Kim, H.J., Lee, E., 2011. Electron flux changes in the outer radiation belt by radial diffusion during the storm recovery phase in comparison with the fully adiabatic evolution. J. Geophys. Res. 116. A09229. https://doi.org/10.1029/2011JA016642.

Kletzing, C.A., Kurth, W.S., Acuna, M., MacDowall, R.J., Torbert, R.B., Averkamp, T., Bodet, D., Bounds, S.R., Chutter, M., Connerney, J., Crawford, D., Dolan, J.S., Dvorsky, R., Hospodarsky, G.B., Howard, J., Jordanova, V., Johnson, R.A., Kirchner, D.L., Mokrzycki, B., Needell, G., Odom, J., Mark, D., Pfaff Jr., R., Phillips, J.R., Piker, C.W., Remington, S.L., Rowland, D., Santolik, O., Schnurr, R., Sheppard, D., Smith, C.W., Thorne, R.M., Tyler, J., 2013. The Electric and Magnetic Field Instrument Suite and Integrated Science (EMFISIS) on RBSP. Space Sci. Rev. 179, 127–181.

Kozyra, J.U., Jordanova, V.K., Borovsky, J.E., Thomsen, M.F., Knipp, D.J., Evans, D.S., McComas, D.J., Cayto, T.E., 1998. Effects of a high-density plasma sheet on ring current development during the November 2–6, 1993, magnetic storm. J. Geophys. Res. 103, 26285–26305.

Kozyra, J.U., Criwley, G., Emery, B.A., Fang, X., Maris, G., Mlynczak, M.G., Niciejewski, R.J., Palo, S.E., Paxton, L.J., Randal, C.E., Rong, P.P., Russell III, J.M., Skinner, W., Solomon, S.C., Talaat, E.R., Wu, Q., Yee, J.H., 2006. Response of the upper/middle atmosphere to coronal holes and powerful high-speed solar wind streams in 2003. In: Tsurutani, B.T., McPherron, R.L., Gonzalez, W.D., Lu, G., Sobral, J.H.A., Gopalswamy, N. (Eds.), Recurrent Magnetic Storms: Corotating Solar Wind Streams. Geophysical Monograph Series, vol. 167. AGU, Washington, DC, pp. 319–340.

Lakhina, G.S., Tsurutani, B.T., Verkhoglyadova, O.P., Pickett, J.S., 2010. Pitch angle transport of electrons due to cyclotron interactions with coherent chorus subelements. J. Geophys. Res. 115. A00F15. https://doi.org/10.1029/2009JA014885.

Li, X., Baker, D.N., Temerin, M.A., Cayton, T.E., Reeves, E.G.D., Christensen, R.A., Blake, J.B., Looper, M.D., Nakamura, R., Kanekal, S.G., 1997. Multi-satellite observations of the outer zone electron variation during the November 3–4, 1993, magnetic storm. J. Geophys. Res. 102, 14123–14140.

Li, X., Temerin, M., Baker, D.N., Reeves, G.D., Larson, G.D., 2001. Quantitative prediction of radiation belt electrons at geostationary orbit based on solar wind measurements. Geophys. Res. Lett. 28, 1887–1890. https://doi.org/10.1029/2000GL012681.

Li, X., Baker, D.N., Elkington, S., Temerin, M., Reeves, G.D., Belian, R.D., Blake, J.B., Singer, H.J., Peria, W., Parks, G., 2003. Energetic particle injections in the inner magnetosphere as a response to an interplanetary shock. J. Atmos. Sol. Terr. Phys. 65, 233–244. https://doi.org/10.1016/S1364-6826(02)00286-9.

Li, X., Baker, D.N., Temerin, M., Reeves, G., Friedel, R., Shen, C., 2005. Energetic electrons, 50 keV to 6 MeV, at geosynchronous orbit: their responses to solar wind variations. Space Weather 3. S04001. https://doi.org/10.1029/2004SW000105.

Li, X., Oh, K.S., Temerin, M., 2007. Prediction of the AL index using solar wind parameters. J. Geophys. Res. 112. A06224. https://doi.org/10.1029/2006JA011918.

Li, W., Thorne, R.M., Bortnik, J., Baker, D.N., Reeves, G.D., Kanekal, S.G., Spence, H.E., Green, J.C., 2015. Solar wind conditions leading to efficient radiation belt electron acceleration: a superposed epoch analysis. Geophys. Res. Lett. 42, 6906–6915. https://doi.org/10.1002/2015GL065342.

Lorentzen, K.R., Blake, J.B., Inan, U.S., Bortnik, J., 2001. Observations of relativistic electron microbursts in association with VLF chorus. J. Geophys. Res. 106, 6017–6027. https://doi.org/10.1029/2000JA003018.

Luo, B., Li, X., Temerin, M., Liu, S., 2013. Prediction of the AU, AL, and AE indices using solar wind parameters. J. Geophys. Res. 118. https://doi.org/10.1002/2013JA019188.

Lyons, L.R., Lee, D.Y., Thorne, R.M., Horne, R.B., Smith, A.J., 2005. Solar wind-magnetosphere coupling leading to relativistic electron energization during high-speed streams. J. Geophys. Res. 110. A11202. https://doi.org/10.1029/2005JA011254.

Mauk, B.H., Fox, N.J., Kanekal, S.G., Kessel, R.L., Sibeck, D.G., Ukhorskiy, A., 2012. Science objectives and rationale for the radiation belt storm probes mission. Space Sci. Rev. 179, 3–27. https://doi.org/10.1007/s11214-012-9908-y.

Mendes, O., Domingues, M.O., Echer, E., Hajra, R., Menconi, V.E., 2017. Characterization of high-intensity, long-duration continuous auroral activity (HILDCAA) events using recurrence quantification analysis. Nonlinear Process. Geophys. 24, 407–417.

Meredith, N.P., Horne, R.B., Anderson, R.R., 2001. Substorm dependence of chorus amplitudes: implications for the acceleration of electrons to relativistic energies. J. Geophys. Res. 106, 13165–13178.

Meredith, N.P., Horne, R.B., Iles, R.H.A., Thorne, R.M., Heynderickx, D., Anderson, R.R., 2002. Outer zone relativistic electron acceleration associated with substorm-enhanced whistler mode chorus. J. Geophys. Res. 107, 1144. https://doi.org/10.1029/2001JA900146.

Meredith, N.P., Cain, M., Horne, R.B., Thorne, R.M., Summers, D., Anderson, R.R., 2003. Evidence for chorus-driven electron acceleration to relativistic energies from a survey of geomagnetically disturbed periods. J. Geophys. Res. 108, 1248. https://doi.org/10.1029/2002JA009764.

Meredith, N.P., Horne, R.B., Glauert, S.A., Thorne, R.M., Summers, D., Albert, J.M., Anderson, R.R., 2006. Energetic outer zone electron loss timescales during low geomagnetic activity. J. Geophys. Res. 111. A05212. https://doi.org/10.1029/2005JA011516.

Miyoshi, Y., Kataoka, R., 2008. Flux enhancement of the outer radiation belt electrons after the arrival of stream interaction regions. J. Geophys. Res. 113. A03S09. https://doi.org/10.1029/2007JA012506.

Miyoshi, Y., Kataoka, R., 2011. Solar cycle variations of outer radiation belt and solar wind structures. J. Atmos. Sol. Terr. Phys. 73 (1), 77–87. https://doi.org/10.1016/j.jastp.2010.09.031.

Miyoshi, Y., Morioka, A., Obara, T., Misawa, T., Nagai, T., Kasahara, Y., 2003. Rebuilding process of the outer radiation belt during the 3 November 1993 magnetic storm: NOAA and Exos-D observations. J. Geophys. Res. 108, 1004. https://doi.org/10.1029/2001JA007542.

Miyoshi, Y., Kataoka, R., Kasahara, Y., Kumamoto, A., Nagai, T., Thomsen, M.F., 2013. High-speed solar wind with southward interplanetary magnetic field causes relativistic electron flux enhancement of the outer radiation belt via enhanced condition of whistler waves. Geophys. Res. Lett. 40, 4520–4525. https://doi.org/10.1002/grl.50916.

Nakamura, R., Isowa, M., Kamide, Y., Baker, D.N., Blake, J.B., Looper, M., 2000. SAMPEX observations of precipitating bursts in the outer radiation belt. J. Geophys. Res. 105, 15875–15885. https://doi.org/10.1029/2000JA900018.

Ness, N.F., Wilcox, J.M., 1964. Solar origin of the interplanetary magnetic field. Phys. Rev. Lett. 13, 461–464.

Ni, B., Xiang, Z., Gu, X., Shprits, Y.Y., Zhou, C., Zhao, Z., Zhang, X., Zuo, P., 2016. Dynamic responses of the Earth's radiation belts during periods of solar wind dynamic pressure pulse based on normalized superposed epoch analysis. J. Geophys. Res. 121, 8523–8536. https://doi.org/10.1002/2016JA023067.

Ohtani, S., Miyoshi, Y., Singer, H.J., Weygand, J.M., 2009. On the loss of relativistic electrons at geosynchronous altitude: its dependence on magnetic configurations and external conditions. J. Geophys. Res. 114. A01202. https://doi.org/10.1029/2008JA013391.

Onsager, T., Grubb, R., Kunches, J., Matheson, L., Speich, D., Zwickl, R.W., Sauer, H., 1996. Operational uses of the GOES energetic particle detectors. In: Proc SPIE 2812, GOES-8 and Beyond 281. https://doi.org/10.1117/12.254075.

Onsager, T.G., Rostoker, G., Kim, H.J., Reeves, G.D., Obara, T., Singer, H.J., Smithtro, C., 2002. Radiation belt electron flux dropouts: local time, radial, and particle-energy dependence. J. Geophys. Res. 107. (A11). https://doi.org/10.1029/2001JA000187.

Paulikas, G.A., Blake, J.B., 1979. Effects of the solar wind magnetospheric dynamics: energetic electrons at the synchronous orbit. In: Olson, W.P. (Ed.), Quantitative Modeling of Magnetospheric Processes. Geophysical Monograph Series, vol. 21. AGU, Washington, DC, p. 180.

Reeves, G.D., McAdams, K.L., Friedel, R.H.W., O'Brien, T.P., 2003. Acceleration and loss of relativistic electrons during geomagnetic storms. Geophys. Res. Lett. 30, 1529. https://doi.org/10.1029/2002GL016513.

Reeves, G.D., Spence, H.E., Henderson, M.G., Morley, S.K., Friedel, R.H.W., Funsten, H.O., Baker, D.N., Kanekal, S.G., Blake, J.B., Fennell, J.F., Claudepierre, S.G., Thorne, R.M., Turner, D.L., Kletzing, C.A., Kurth, W.S., Larsen, B.A., Niehof, J.T., 2013. Electron acceleration in the heart of the Van Allen radiation belts. Science 341, 991–994. https://doi.org/10.1126/science.1237743.

Reeves, G.D., Friedel, R.H.W., Larsen, B.A., Skoug, R.M., Funsten, H.O., Claudepierre, S.G., Fennell, J.F., Turner, D.L., Denton, M.H., Spence, H.E., Blake, J.B., Baker, D.N., 2016. Energy dependent dynamics of keV to MeV electrons in the inner zone, outer zone, and slot regions. J. Geophys. Res. 121, 397–412. https://doi.org/10.1002/2015JA021569.

Roederer, J.G., Zhang, H., 2014. Dynamics of Magnetically Trapped Particles—Foundations of the Physics of Radiation Belts and Space Plasmas. Springer, Heidelberg/New York/Dordrecht/London.

Roth, I., Temerin, M.A., Hudson, M.K., 1999. Resonant enhancement of relativistic electron fluxes during geomagnetically active periods. Ann. Geophys. 17, 631–638.

Santolik, O., Macusova, E., Kolmasova, I., Cornilleau-Wehrlin, N., de Conchy, Y., 2014. Propagation of lower-band whistler-mode waves in the outer Van Allen belt: systematic analysis of 11 years of multi-component data from the Cluster spacecraft. Geophys. Res. Lett. 41, 2729–2737.

Schulz, M., Lanzerotti, L., 1974. Particle Diffusion in the Radiation Belts. Springer, New York.

Selesnick, R.S., 2015. High-energy radiation belt electrons from CRAND. J. Geophys. Res. 120, 2912–2917. https://doi.org/10.1002/2014JA020963.

Selesnick, R.S., Blake, J.B., 2000. On the source location of radiation belt relativistic electrons. J. Geophys. Res. 105, 2607–2624. https://doi.org/10.1029/1999JA900445.

Selesnick, R.S., Su, Y.J., Blake, J.B., 2016. Control of the innermost electron radiation belt by large-scale electric fields. J. Geophys. Res. 121, 8417–8427. https://doi.org/10.1002/2016JA022973.

Sheeley Jr., N.R., Harvey, J.W., Feldman, W.C., 1976. Coronal holes, solar wind streams and recurrent geomagnetic disturbances: 1973–1976. Sol. Phys. 49, 271–278.

Shprits, Y.Y., Thorne, R.M., Friedel, R., Reeves, G.D., Fennell, J., Baker, D.N., Kanekal, S.G., 2006. Outward radial diffusion driven by losses at magnetopause. J. Geophys. Res. 111. A11214. https://doi.org/10.1029/2006JA011657.

Singer, S.F., 1958. Trapped albedo theory of the radiation belt. Phys. Rev. Lett. 1, 181–183.

Smith, E.J., 1985. Interplanetary shock phenomena beyond 1 AU. In: Tsurutani, B.T., Stone, R.G. (Eds.), Collisionless Shocks in the Heliosphere: Reviews of Current Research. Geophysical Monograph Series, vol. 35. AGU, Washington, DC, p. 69. https://doi.org/10.1029/GM035p0069.

Smith, E.J., Wolfe, J.H., 1976. Observations of interaction regions and corotating shocks between one and five AU: pioneers 10 and 11. Geophys. Res. Lett. 3, 137–140. https://doi.org/10.1029/GL003i003p00137.

Smith, E.J., Tsurutani, B.T., Rosenberg, R.L., 1978. Observations of the interplanetary sector structure up to heliographic latitudes of 16°: pioneer 11. J. Geophys. Res. 83, 717–724.

Soraas, F., Oksavik, K., Aarsnes, K., Evans, D.S., Greer, M.S., 2003. Storm time equatorial belt—an "image" of RC behavior. Geophys. Res. Lett. 30. https://doi.org/10.1029/2002GL015636.

Souza, A.M., Echer, E., Bolzan, M.J.A., Hajra, R., 2016. A study on the main periodicities in interplanetary magnetic field Bz component and geomagnetic AE index during HILDCAA events using wavelet analysis. J. Atmos. Sol. Terr. Phys. 149, 81–86.

Su, Y.J., Selesnick, R.S., Blake, J.B., 2016. Formation of the inner electron radiation belt by enhanced large-scale electric fields. J. Geophys. Res. 121, 8508–8522. https://doi.org/10.1002/2016JA022881.

Summers, D., Thorne, R.M., 2003. Relativistic pitch angle scattering by electromagnetic ion cyclotron waves during geomagnetic storms. J. Geophys. Res. 108, 1143. https://doi.org/10.1029/2002JA009489.

Summers, D., Thorne, R.M., Xiao, F., 1998. Relativistic theory of wave-particle resonant diffusion with application to electron acceleration in the magnetosphere. J. Geophys. Res. 103, 20487–20500. https://doi.org/10.1029/98JA01740.

Summers, D., Ma, C., Meredith, N.P., Horne, R.B., Thorne, R.M., Heynderickx, D., Anderson, R.R., 2002. Model of the energization of outer-zone electrons by whistler-mode chorus during the October 9, 1990 geomagnetic storm. Geophys. Res. Lett. 29, 2174. https://doi.org/10.1029/2002GL016039.

Summers, D., Ma, C., Meredith, N.P., Horne, R.B., Thorne, R.M., Anderson, R.R., 2004. Modeling outer-zone relativistic electron response to whistler mode chorus activity during substorms. J. Atmos. Sol. Terr. Phys. 66, 133–146.

Summers, D., Mace, R.L., Hellberg, M.A., 2005. Pitch-angle scattering rates in planetary magnetospheres. J. Plasma Phys. 71, 237–250.

Summers, D., Ni, B., Meredith, N.P., 2007. Timescale for radiation belt electron acceleration and loss due to resonant wave-particle interactions: 2. Evaluation for VLF chorus, ELF hiss, and electromagnetic ion cyclotron waves. J. Geophys. Res. 112. A04207. https://doi.org/10.1029/2006JA011993.

Temerin, M., Li, X., 2006. Dst model for 1995–2002. J. Geophys. Res. 111. A04221. https://doi.org/10.1029/2005JA011257.

Thorne, R.M., Kennel, C.F., 1971. Relativistic electron precipitation during magnetic storm main phase. J. Geophys. Res. 76, 4446–4453. https://doi.org/10.1029/JA076i019p04446.

Thorne, R.M., O'Brien, T.P., Shprits, Y.Y., Summers, D., Horne, R.B., 2005. Timescale for MeV electron microburst loss during geomagnetic storms. J. Geophys. Res. 110. A09202. https://doi.org/10.1029/2004JA010882.

Thorne, R.M., Li, W., Ni, B., Ma, Q., Bortnik, J., Chen, L., Baker, D.N., Spence, H.E., Reeves, G.D., Henderson, M.G., Kletzing, C.A., Kurth, W.S., Hospodarsky, G.B., Blake, J.B., Fennell, J.F., Claudepierre, S.G., Kanekal, S.G., 2013. Rapid local acceleration of relativistic radiation-belt electrons by magnetospheric chorus. Nature 504, 411–414.

Tsurutani, B.T., Gonzalez, W.D., 1987. The cause of high-intensity long-duration continuous AE activity (HILDCAAs): interplanetary Alfvén wave trains. Planet. Space Sci. 35, 405–412.

Tsurutani, B.T., Lakhina, G.S., 1997. Some basic concepts of wave-particle interactions in collisionless plasmas. Rev. Geophys. 35, 491–501. https://doi.org/10.1029/97RG02200.

Tsurutani, B.T., Lin, R.P., 1985. Acceleration of >47 keV ions and >2 keV electrons by interplanetary shocks at 1 AU. J. Geophys. Res. 90, 1–11. https://doi.org/10.1029/JA090iA01p00001.

Tsurutani, B.T., Smith, E.J., 1974. Magnetospheric ELF (10-1000 Hz) electromagnetic-waves during storms and substorms. Trans. Am. Geophys. Union 55, 1019.

Tsurutani, B.T., Smith, E.J., 1977. Two types of magnetospheric ELF chorus and their substorm dependences. J. Geophys. Res. 82, 5112–5128. https://doi.org/10.1029/JA082i032p05112.

Tsurutani, B.T., Smith, E.J., West Jr., H.I., Buck, R.M., 1979. Chorus, energetic electrons and magnetospheric substorms. In: Palmadesso, P.J., Papadopoulos, K. (Eds.), Wave Instabilities in Space Plasmas. D. Reidel, Dordrecht, p. 55.

Tsurutani, B.T., Gonzalez, W.D., Tang, F., Akasofu, S.I., Smith, E.J., 1988. Origin of interplanetary southward magnetic fields responsible for major magnetic storms near solar maximum (1978–1979). J. Geophys. Res. 93, 8519–8531. https://doi.org/10.1029/JA093iA08p08519.

Tsurutani, B.T., Ho, C.M., Smith, E.J., Neugebauer, M., Goldstein, B.E., Mok, J.S., Arballo, J.K., Balogh, A., Southwood, D.J., Feldman, W.C., 1994. The relationship between interplanetary discontinuities and Alfvén waves: Ulysses observations. Geophys. Res. Lett. 21, 2267–2270. https://doi.org/10.1029/94GL02194.

Tsurutani, B.T., Gonzalez, W.D., Gonzalez, A.L.C., Tang, F., Arballo, J.K., Okada, M., 1995. Interplanetary origin of geomagnetic activity in the declining phase of the solar cycle. J. Geophys. Res. 110, 21717–21733.

Tsurutani, B.T., Gonzalez, W.D., Guarnieri, F., Kamide, Y., Zhou, X., Arballo, J.K., 2004. Are high-intensity long-duration continuous AE activity (HILDCAA) events substorm expansion events? J. Atmos. Sol. Terr. Phys. 66, 167–176.

Tsurutani, B.T., Gonzalez, W.D., Gonzalez, A.L.C., Guarnieri, F.L., Gopalswamy, N., Grande, M., Kamide, Y., Kasahara, Y., Lu, G., McPherron, R.L., Soraas, F., Vasyliunas, V., 2006. Corotating solar wind streams and recurrent geomagnetic activity: a review. J. Geophys. Res. 111. A07S01. https://doi.org/10.1029/2005JA011273.

Tsurutani, B.T., Verkhoglyadova, O.P., Lakhina, G.S., Yagitani, S., 2009. Properties of dayside outer zone chorus during HILDCAA events: loss of energetic electrons. J. Geophys. Res. 114. A03207. https://doi.org/10.1029/2008JA013353.

Tsurutani, B.T., Lakhina, G.S., Verkhoglyadova, O.P., Gonzalez, W.D., Echer, E., Guarnieri, F.L., 2011. A review of interplanetary discontinuities and their geomagnetic effects. J. Atmos. Sol. Terr. Phys. 73, 5–19. https://doi.org/10.1016/j.jastp.2010.04.001.

Tsurutani, B.T., Lakhina, G.S., Verkhoglyadova, O.P., 2013. Energetic electron (>10 keV) microburst precipitation, ~5-15 s X-ray pulsations, chorus, and wave-particle interactions: a review. J. Geophys. Res. 118, 2296–2312. https://doi.org/10.1002/jgra.50264.

Tsurutani, B.T., Hajra, R., Tanimori, T., Takada, A., Bhanu, R., Mannucci, A.J., Lakhina, G.S., Kozyra, J.U., Shiokawa, K., Lee, L.C., Echer, E., Reddy, R.V., Gonzalez, W.D., 2016. Heliospheric plasma sheet (HPS) impingement onto the magnetosphere as a cause of relativistic electron dropouts (REDs) via coherent EMIC wave scattering with possible consequences for climate change mechanisms. J. Geophys. Res. 121, 10130–10156. https://doi.org/10.1002/2016JA022499.

Turner, D.L., Li, X., 2008. Quantitative forecast of relativistic electron flux at geosynchronous orbit based on low-energy electron flux. Space Weather 6. S05005. https://doi.org/10.1029/2007SW000354.

Turner, N.E., Mitchell, E.J., Knipp, D.J., Emery, B.A., 2006. Energetics of magnetic storms driven by corotating interaction region: a study of geoeffectiveness. In: Tsurutani, B.T., McPherron, R.L., Gonzalez, W.D., Lu, G., Sobral, J.H.A., Gopalswamy, N. (Eds.), Recurrent Magnetic Storms: Corotating Solar Wind Streams. Geophysical Monograph Series, vol. 167. AGU, Washington, DC, pp. 113–124.

Turner, D.L., Angelopoulos, V., Li, W., Hartinger, M.D., Usanova, M., Mann, I.R., Bortnik, J., Shprits, Y., 2013. On the storm-time evolution of relativistic electron phase space density in Earth's outer radiation belt. J. Geophys. Res. 118, 2196–2212. https://doi.org/10.1002/jgra.50151.

Turner, D.L., Angelopoulos, V., Li, W., Bortnik, J., Ni, B., Ma, Q., Thorne, R.M., Morley, S.K., Henderson, M.G., Reeves, G.D., Usanova, M., Mann, I.R., Claudepierre, S.G., Blake, J.B., Baker, D.N., Huang, C.L., Spence, H., Kurth, W., Kletzing, C., Rodriguez, J.V., 2014. Competing source and loss mechanisms due to wave-particle interactions in Earth's outer radiation belt during the 30 September to 3 October 2012 geomagnetic storm. J. Geophys. Res. 119, 1960–1979. https://doi.org/10.1002/2014JA019770.

Ukhorskiy, A.Y., Anderson, B.J., Brandt, P.C., Tsyganenko, N.A., 2006. Storm time evolution of the outer radiation belt: transport and losses. J. Geophys. Res. 111. A11S03. https://doi.org/10.1029/2006JA011690.

Usanova, M.E., Drozdov, A., Orlova, K., Mann, I.R., Shprits, Y., Robertson, M.T., Turner, D.L., Milling, D.K., Kale, A., Baker, D.N., Thaller, S.A., Reeves, G.D., Spence, H.E., Kletzing, C., Wygant, J., 2014. Effect of EMIC waves on relativistic and ultrarelativistic electron populations: ground-based and Van Allen Probes observations. Geophys. Res. Lett. 41, 1375–1381. https://doi.org/10.1002/2013GL059024.

Van Allen, J.A., Frank, L.A., 1959. Radiation measurements to 658,300 km with Pioneer IV. Nature 184, 219–224.

Vernov, S.N., Chudakov, A.E., Vakulov, P.V., Logachev, Y.I., Nikolayev, A.G., 1960. Radiation measurements during the flight of the second Soviet space rocket. In: Kallmann-Bijl, H. (Ed.), Space Research: Proceedings of the First International Space Science Symposium. North-Holland Publications, Amsterdam, p. 845.

West Jr., H.I., Buck, R.M., Walton, J.R., 1972. Shadowing of electron azimuthal-drift motions near the noon magnetopause. Nature Phys. Sci. 240, 6–7. https://doi.org/10.1038/physci240006a0.

West Jr., H.I., Buck, R.M., Davidson, G.T., 1981. The dynamics of energetic electrons in the Earth's outer radiation belt during 1968 as observed by the Lawrence Livermore National Laboratory's Spectrometer on Ogo 5. J. Geophys. Res. 86, 2111–2142. https://doi.org/10.1029/JA086iA04p02111.

Winterhalter, D., Smith, E.J., Burton, M.E., Murphy, N., McComas, D.J., 1994. The heliospheric plasma sheet. J. Geophys. Res. 99, 6667–6680.

Wrenn, G.L., 1995. Conclusive evidence for internal dielectric charging anomalies on geosynchronous communications spacecraft. J. Spacecr. Rocket. 32, 514–520. https://doi.org/10.2514/3.26645.

Wygant, J.R., Bonnell, J.W., Goetz, K., Ergun, R.E., Mozer, F.S., Bale, S.D., Ludlam, M., Turin, P., Harvey, P.R., Hochmann, R., Harps, K., Dalton, G., McCauley, J., Rachelson, W., Gordon, D., Donakowski, B., Shultz, C., Smith, C., Diaz-Aguado, M., Fischer, J., Heavner, S., Berg, P., Malsapina, D.M., Bolton, M.K., Hudson, M., Strangeway, R.J., Baker, D.N., Li, X., Albert, J., Foster, J.C., Chaston, C.C., Mann, I., Donovan, E., Cully, C.M., Cattell, C.A., Krasnoselskikh, V., Kersten, K., Brenneman, A., Tao, J.B., 2013. The electric field and waves instruments on the radiation belt storm probes mission. Space Sci. Rev. 179, 183–220.

Xie, L., Pu, Z.Y., Zhou, X.Z., Fu, S.Y., Zong, Q.G., Hong, M.H., 2006. Energetic ion injection and formation of the storm-time symmetric ring current. Ann. Geophys. 24, 3547–3556.